# Chapter 12
# Further Applications of the Fourier Transform

**Abstract** Further applications of Fourier analysis are examined. Shannon's sampling theorem is proven and discussed. The spectral properties of sampling applications are considered and a basic digital transmission system is shown. The transmission of signals with a linear multi-carrier system, such as WLAN or mobile data transmission, is treated as a current everyday application. The method is orthogonal frequency division multiplexing (OFDM), which uses the FFT and linear filters. Further sections examine the Heisenberg uncertainty principle and its consequences for the time-bandwidth product of signals. Closely related to this is the windowed Fourier transform (STFT) as a tool for time-frequency analysis. Inversion formulas for the STFT with continuous and discrete parameters are proven. The use of time windows in the DFT to reduce alias effects is discussed. In further sections, initial value problems for the homogeneous and inhomogeneous wave and heat equations in two and three dimensions are solved. The Fourier transform of distributions is used to solve these equations. The Huygens' principle for waves is explained. For the heat equation, an inhomogeneous boundary value 3D problem is solved approximately as a further application of the FEM method and the solution is displayed graphically.

## 12.1 Shannon's Sampling Theorem

The theoretical starting point for signal transmission methods, where discrete approximations of $f(t)$ are transmitted instead of a continuous analog signal $f(t)$, is Shannon's sampling theorem (1949). It states that a signal $f(t)$ can be reconstructed from its samples under suitable conditions. A recommended read on the history of the theorem and its developments, with a wealth of relevant references, is the article "*Sampling – 50 Years After Shannon*" by M. Unser (2000).

## Shannon's Sampling Theorem for Bandlimited Functions

**Theorem 12.1** (Sampling Theorem)**.** *If $f$ is an integrable function that is bandlimited by $\omega_c > 0$ , i.e., $\widehat{f}(\omega) = 0$ for $|\omega| > \omega_c$, and if $tf(t)$ is also integrable with $f(t)$, then for all $t \in \mathbb{R}$ with $t_a = \pi/\omega_c$, the following sampling formula holds:*

$$f(t) = \sum_{k=-\infty}^{+\infty} f\left(\frac{k\pi}{\omega_c}\right) \frac{\sin(\omega_c t - k\pi)}{\omega_c t - k\pi} = \sum_{k=-\infty}^{+\infty} f\left(kt_a\right) \frac{\sin(\omega_c(t - kt_a))}{\omega_c(t - kt_a)},$$

*the series being absolutely and uniformly convergent.*

*Proof.* From the assumptions, it follows that the spectral function $\widehat{f}$ is continuously differentiable (cf. p.262). Hence, it is represented pointwise by its Fourier series in $[-\omega_c, \omega_c]$ and this series is absolutely and uniformly convergent (cf. p.26):

$$\widehat{f}(\omega) = \sum_{k=-\infty}^{+\infty} c_k \, \mathrm{e}^{-jk\omega t_a} \qquad (t_a = \pi/\omega_c,\ |\omega| \leqslant \omega_c)$$

$$c_k = \frac{1}{2\omega_c} \int_{-\omega_c}^{+\omega_c} \widehat{f}(\omega) \, \mathrm{e}^{jk\omega t_a} \, \mathrm{d}\omega = \frac{\pi}{\omega_c} f(kt_a).$$

Term-by-term integration of the series is possible because the series converges uniformly. Since bandlimited functions are infinitely differentiable (cf. p. 262), the sampling theorem follows from the Fourier inversion formula:

$$f(t) = \frac{1}{2\pi} \int_{-\omega_c}^{+\omega_c} \widehat{f}(\omega) \, \mathrm{e}^{j\omega t} \, \mathrm{d}\omega = \frac{1}{2\pi} \int_{-\omega_c}^{+\omega_c} \sum_{k=-\infty}^{+\infty} c_k \, \mathrm{e}^{-jk\omega t_a} \, \mathrm{e}^{j\omega t} \, \mathrm{d}\omega$$

$$= \sum_{k=-\infty}^{+\infty} \frac{1}{2\omega_c} f(kt_a) \int_{-\omega_c}^{+\omega_c} \mathrm{e}^{j\omega(t-kt_a)} \, \mathrm{d}\omega = \sum_{k=-\infty}^{+\infty} f\left(\frac{k\pi}{\omega_c}\right) \frac{\sin(\omega_c t - k\pi)}{\omega_c t - k\pi}.$$

□

**Remark.** As a reference for variants and generalizations of the theorem, see A. Jerri (1977) or P. L. Butzer, R. L. Stens, W. Splettstößer (1988). For example, with theorems of R. Paley, N. Wiener (1934) it can be shown that the sampling series converges absolutely and uniformly for band-limited square-integrable functions.

The sampling theorem provides a formula that allows for the interpolation of the values of $f$ at times $t \neq k\pi/\omega_c$, given all discrete values $f(k\pi/\omega_c)$, $k \in \mathbb{Z}$. The sampling frequency must be at least twice the cut-off frequency $\omega_c/(2\pi)$. By increasing the sampling frequency $\omega_c/\pi$, the formula applies to signals of correspondingly higher frequency bandwidth. With a lower sampling frequency than $\omega_c/\pi$ and given bandwidth $\omega_c$ of $f$, aliasing effects occur with the sampling series (see p. 360).

For direct practical implementation in signal transmission, the formula is not suitable because it is not causal. To reconstruct $f(t_0)$ at time $t_0$, one would also need all values $f(k\pi/\omega_c)$, $k\pi/\omega_c > t_0$. However, a function $f$ whose spectrum $\widehat{f}$ vanishes outside an interval $[-\omega_c, \omega_c]$ is not time-limited (cf. p. 281), meaning the sampling formula requires non-zero values of $f$ from the entire future $t > t_0$. Nevertheless, the sampling theorem is a starting point for practical approximation methods for reconstructing $f$ from sample values. In these methods, a realizable filter for interpolation is used, replacing the impulse response of the ideal low-pass filter used below.

To illustrate, consider finitely many samples $f(k\pi/\omega_c)$, $-M \leqslant k \leqslant N$. Form the impulse sequence $\dfrac{\pi}{\omega_c} \displaystyle\sum_{k=-M}^{+N} f\left(k\frac{\pi}{\omega_c}\right) \delta\left(t - k\frac{\pi}{\omega_c}\right)$ as the input signal for an ideal low-pass filter with the frequency response $\widehat{h}(\omega) = A_0\,\mathrm{e}^{-j\omega t_0}$ for $|\omega| \leqslant \omega_c$, $\widehat{h}(\omega) = 0$ for $|\omega| > \omega_c$, then at the output of the low-pass filter we get (see Fig. 12.1)

$$\begin{aligned}
&\frac{\pi}{\omega_c} \sum_{k=-M}^{+N} f\left(k\frac{\pi}{\omega_c}\right) \delta\left(t - \frac{k\pi}{\omega_c}\right) * \frac{A_0 \sin\left(\omega_c(t-t_0)\right)}{\pi(t-t_0)} \\
&= A_0 \sum_{k=-M}^{+N} f\left(k\frac{\pi}{\omega_c}\right) \frac{\sin\left(\omega_c(t-t_0) - k\pi\right)}{\omega_c(t-t_0) - k\pi}.
\end{aligned}$$

Except for a factor and the time delay of $t_0$, the right side is an approximation of $f$ that converges to $A_0 f(t-t_0)$ as $N, M \to \infty$.

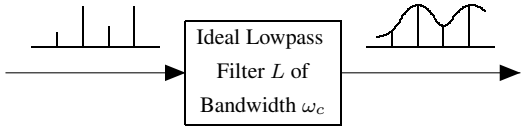


$$\frac{\pi}{\omega_c} \sum_{k=-M}^{+N} f\left(k\frac{\pi}{\omega_c}\right) \delta\left(t - k\frac{\pi}{\omega_c}\right) \xrightarrow{\quad L \quad} A_0 \sum_{k=-M}^{+N} f\left(k\frac{\pi}{\omega_c}\right) \frac{\sin\Big(\omega_c(t-t_0) - k\pi\Big)}{\omega_c(t-t_0) - k\pi}$$

**Fig. 12.1.** Schematic digital to analog conversion

**Remarks.** 1) The functions $e_k(t) = \sqrt{\dfrac{\omega_c}{\pi}} \dfrac{\sin(\omega_c t - k\pi)}{\omega_c t - k\pi}$ ($k \in \mathbb{Z}$) form a complete orthonormal system in the space of $L^2$ functions bandlimited by $\omega_c$. The sampling formula is thus precisely the development of $f$ with respect to these basis functions. The proof of the sampling theorem shows that $\widehat{e_k}(\omega) = \sqrt{\pi/\omega_c}\,\mathrm{e}^{-j\omega k\pi/\omega_c}$ holds for $|\omega| \leqslant \omega_c$, $\widehat{e_k}(\omega) = 0$ otherwise. Completeness and orthogonality of the functions $e_k(t)$ therefore follow from Plancherel's equation (p. 286) and the fact that the functions $\widehat{e_k}(\omega)$ form a complete orthogonal system in $L^2([-\omega_c, \omega_c])$.

2) The sampling series converges very slowly because the interpolation function $\sin(t)/t$ decays slowly for $|t| \to \infty$. With oversampling, i.e., replacing the sampling points $k\pi/\omega_c$ by $k\pi/(\alpha\omega_c)$ with $\alpha > 1$, one can obtain an interpolation function

that decays like $1/t^2$ for $|t| \to \infty$. To see this precisely, solve the corresponding exercise A1 in the exercise part 12.9.

3) With additional assumptions about $f$, such as information about the energy distribution of $f$ or its decay behavior, error estimates for the truncation error of the above approximation can be shown. Similarly, there are error estimates for the case when the sampling points are not exactly maintained and instead of $f(k\pi/\omega_c)$ the values $f(k\pi/\omega_c + \varepsilon_k)$ are sampled (so-called jitter errors). In addition, in practical transmission systems, the sampled values are not transmitted continuously but the value range is discretized and only a finite number of rounded values are transmitted. The resulting signal distortion, called quantization noise, corresponds in the time domain to the addition of an impulse train with the consequence of a broadband noise spectrum. There are also studies on the rounding errors resulting from this. For readers interested in error analysis, it is recommended to start with works such as A. Jerri (1977).

4) Sampling methods with irregularly distributed sampling points (irregular sampling) play a role, for example, in radar technology. For this, see the works of H.-G. Feichtinger and K. Gröchenig (detailed references can be found in M. Unser (2000)).

*Generalizations*

There are numerous generalizations of the presented sampling theorem. These include, in particular, sampling theorems for time-limited, generally non-bandlimited functions with statements about the approximation quality of the considered sampling series. In general, representations of the form

$$f(t) = \sum_{k\in\mathbb{Z}} f\left(k\frac{\pi}{\Omega}\right)\varphi(\Omega t - k\pi) \quad \text{or} \quad f(t) = \lim_{\Omega\to\infty} \sum_{k\in\mathbb{Z}} f\left(k\frac{\pi}{\Omega}\right)\varphi(\Omega t - k\pi)$$

are sought for functions $f$ of certain function classes and a bandwidths $\Omega$, and the approximation properties of the sampling series are derived from the assumptions about the function $f$ and the properties of the kernels $\varphi$. Such properties can be time- or bandlimitation, decay behavior, etc. This topic will not be further addressed here, but rather reference is made to further literature such as P. L. Butzer, R. L. Stens (1992) or M. Unser (2000) and the references cited therein. Further aspects can also be found in the following Sections 12.5 on time-frequency analysis (see p. 387) and Section 14.2 on wavelets (see p. 437).

## 12.2 Sampling as the Basis of Digital Transmission Technology

**Sampling, Critical Sampling, Over- and Undersampling**.

Equidistant sampling of a bandlimited - and therefore infinitely differentiable - slowly increasing function $f \in \mathcal{O}_M$, with a sampling frequency $1/t_a$ can be described as the multiplication of $f$ with a sequence of impulses at the times $kt_a$. With

the note on p. 150 and impulse strengths $t_a f(kt_a)$ the resulting discrete signal $f_d$ and $f$ as well as $\widehat{f}_d$ and $\widehat{f}$ each have the same physical units (see also p. 362 for the reconstruction of $f$ from sampled values or literature on the functionality of D/A converters for voltage signals in volts). For $f_d$ – understood as a distribution with time parameter $t$ – the following applies

$$f_d(t) = f(t) \cdot \sum_{k=-\infty}^{+\infty} t_a \delta(t - kt_a) = t_a \sum_{k=-\infty}^{+\infty} f(kt_a)\delta(t - kt_a).$$

Therefore, from the theorems on the convergence of convolutions (p. 182) and on Fourier transforms of impulse trains (p. 276) and of products (p. 279), the following fundamental relationship between the spectrum $\widehat{f}$ of $f$ and the periodic spectrum of the discrete signal $f_d$ follows (cf. 323):

**Theorem 12.2.** *The spectrum of the discrete signal $f_d$, which is generated by sampling a bandlimited function $f \in \mathcal{O}_M$ with sampling frequency $1/t_a$, is given by*

$$\widehat{f}_d(\omega) = \widehat{f} * \sum_{k=-\infty}^{+\infty} \delta(\omega - 2\pi k/t_a) = \sum_{k=-\infty}^{+\infty} \widehat{f}(\omega - 2\pi k/t_a).$$

For $k \neq 0$, the spectra $\widehat{f}(\omega - 2\pi k/t_a)$ are *replicas* of $\widehat{f}$. In the case of *critical sampling* with the sampling rate $1/t_a = \omega_c/\pi$, referred to as the *Nyquist frequency*, these replicated spectra immediately adjoin each other. A reconstruction of $f$ from the sample values using a realizable low-pass filter is generally not possible, as this requires a transition region from the passband to the stopband (cf. p. 313). This transition region only arises at sampling rates $1/t_a > \omega_c/\pi$, i.e., through *oversampling* (Fig. 12.2). In the case of *undersampling* with rates $1/t_a < \omega_c/\pi$, overlaps of the replicated spectra occur in the spectrum of $f_d$. A reconstruction of $f$ from the corresponding sample values is then not possible, as aliasing effects occur in the signal spectrum, especially at higher frequencies (Fig. 12.3). The following schematic diagram shows the first graphic as a magnitude spectrum of $f_d$ with oversampling $t_a < \pi/\omega_c$, the second as a magnitude spectrum of $f_d$ with undersampling $t_a > \pi/\omega_c$.

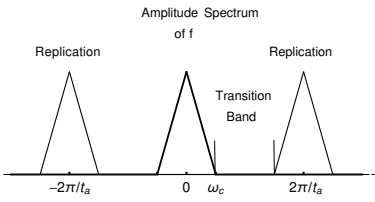


**Fig. 12.2.** Sampling without aliasing

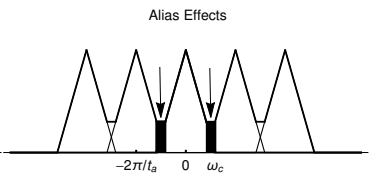


**Fig. 12.3.** Sampling with aliasing

### The Scheme of Digital Transmission in Practice

In practical implementations, the sampling theorem suggests the recipe that low-pass filtering of the impulse sequence obtained from the sample values yields an approximation of the continuous signal. An impression is given by the following diagram. Sampling is technically done through sample and hold circuits ($S\&H$). The values of the resulting step function are proportional to the quantized sample values of the signal. The impulse sequence for *reconstruction* from the quantized sample values is approximated by a sequence of rectangular pulses. An impulse $\delta(t - kt_a)$ at sampling frequency $FS = 1/t_a$ (*DAC sampling frequency clock* $FS$) is replaced by the rectangle $R(t-kt_a)/t_a$, $R$ being the indicator function of $[0\,,\,t_a\,[$ ("rectangle area" equal to one), i.e., an impulse $t_a\delta(t - kt_a)$ of strength $t_a$ is replaced by the convolution $t_a\delta(t - kt_a) * R(t)/t_a = R(t - kt_a)$. This creates a step function with the quantized sample values, i.e., in addition to quantization errors, there are distortions compared to the spectrum of the discrete signal model $f_d$, as the spectrum $t_a\,\mathrm{e}^{-j\omega kt_a}$ of an impulse $t_a\delta(t - kt_a)$ is multiplied by the spectrum $\mathrm{e}^{-j\omega t_a/2}\,\sin(\omega t_a/2)/(\omega t_a/2)$ of the rectangle $R(t)/t_a$ (cf. p. 254). These distortions can be compensated by a correction filter (*inverse* $\sin(x)/x$ *filter*) with digital filtering before the D/A conversion or afterwards with an analog filter (see Fig. 12.4).

Specifically, for example, in digital telephony with ISDN, and similarly in newer methods like Voice over IP, a frequency range up to 3700 Hz is transmitted, and filtered with a stopband starting at 4000 Hz. In standard telephone quality, speech signals are sampled at 8 kHz according to the sampling theorem, i.e., at time intervals of 125 $\mu$s. Only quantized, rounded values are transmitted, which can be encoded as 8-bit long digital code words. In Voice over IP, optionally lossy compressions are also used, similar to the MP3 encoding mentioned later, i.e., code words with less than 8 bits per sample value are used to ultimately reduce the required bandwidth during transmission.

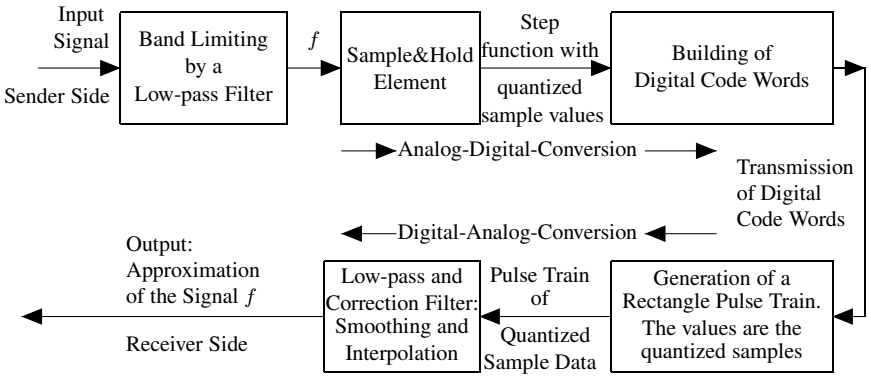


**Fig. 12.4.** Illustratively a digital transmission system

In the European PCM30 system (PCM stands for Pulse Code Modulation) for landline connections, 32 channels per transmission device are transmitted in a bit frame of $32 \times 8\,\mathrm{bit} = 256\,\mathrm{bit}$ per pulse frame, i.e., every 125 $\mu$s. One of the 32

channels contains a frame synchronization word, another channel contains signaling information (e.g., dialed phone numbers), and the remaining 30 channels contain the voice signals of 30 different conversations, which can be transmitted over shared line routes through cyclic aggregation (multiplexing) (see the following graphic for a PCM30 bit frame).

The simultaneous transmission of multiple signals over a shared line between switching centers is possible through time utilization between the sampling points of a signal. During this time, other signals are sampled and transmitted. In this technique, the bit rate per telephone channel is $8 \times 8\,000\,\mathrm{bit} = 64\,\mathrm{kbit/s}$, resulting in a bit rate for the transmission device for 32 channels of $32 \times 64\,\mathrm{kbit/s} = 2.048\,\mathrm{Mbit/s}$ (see Fig. 12.5). The economic benefit in digital telephony is an increase in switching capacity and the high utilization of expensive lines between the switching centers. This technology is still in use but is increasingly being replaced by the aforementioned Internet telephony, which saves costs for operators through higher bandwidth usage and cheaper equipment in the switching centers.

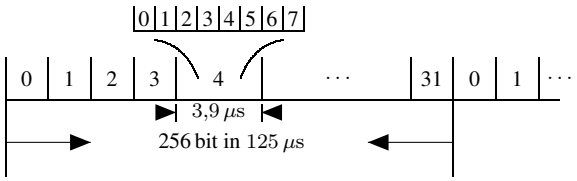


**Fig. 12.5.** PCM30 bit frame with 8-bit code word per sample of the conversation on channel 4

A well-known additional application example of the sampling theorem is audio files in the so-called WAV format. Here, sampling is done with 44100 values per second, i.e., a bandwidth of about 20 kHz is achieved. In the MP3 format, the frequency range is divided into several sub-bands. The FFT values of time sections of the acoustic signal are then quantized and transmitted with a varying number of bits based on psychoacoustic criteria depending on the location in the frequency range. At the receiver, an approximation of the signal is reconstructed from these spectral values. Details on this can be quickly found in an MP3 specification if interested.

### Modulation with Nyquist Pulses

The starting point of discrete signal processing in today's digital transmission methods are discrete values $x_k$, $k \in \mathbb{Z}$, in which the useful information is transported. In the mathematical model, an impulse sequence $x_d = t_a \sum_{k\in\mathbb{Z}} x_k \delta_k = t_a \sum_{k\in\mathbb{Z}} x_k \delta(t - kt_a)$ is present, from which a continuous signal $s = x_d * h$ is generated through a linear filter with regular impulse response $h$. We assume that the convolution $x_d * h$ is possible and all sampling values $h(nt_a)$ exist (e.g., $\mathrm{supp}(x_d)$ bounded, $h \in \mathcal{S}'$ continuous).

$$s(t) = (x_d * h)(t) = \sum_{k\in\mathbb{Z}} x_k t_a h(t - kt_a).$$

With $h$, the transmission and reception filters and a linear filter describing the transmission channel are combined, i.e., $s(t)$ is the received signal. It is immediately apparent that the sampling values $s(nt_a) = x_n$ yield exactly the desired useful information if $t_a h(0) = 1$ and $h(nt_a) = 0$ for $n \neq 0$. Filters $h$, also called *pulse shapes* with this property (*zero crossing property*) are called *Nyquist Pulses*.

**Example.** If the values $x_k$ are sampled values $x_k = f(kt_a)$ of a function $f$ bandlimited by $\omega_c$ as in the previous Shannon sampling theorem and the function $h(t) = \dfrac{\sin(\omega_c t)}{\pi t}$ with $\omega_c = \pi/t_a$, then according to the proof of the sampling theorem $s(t) = f(t)$. The function $h$ is a Nyquist pulse, as are products of $h$ with functions $g$ that have the value $g(0) = 1$ at zero. The so-called "*raised cosine filter*" $h_{\mathrm{RC},\alpha}$, which in practice is often used and falls off much faster than $h$ for $|t| \to \infty$, is an example of this (see also later on p. 371, where it is given as a pulse shape in the frequency domain):

$$h_{\mathrm{RC},\alpha}(t) = \frac{\sin(\pi t/t_a)}{\pi t} \cdot \frac{\cos(\pi\alpha t/t_a)}{1 - (2\alpha t/t_a)^2}.$$

The parameter $\alpha$ controls the bandwidth extension (*excess bandwidth*) compared to the spectrum of the sinc pulse $h$. The spectrum $\widehat{h}_{\mathrm{RC},\alpha}$ with falling cosine flanks, from which this pulse shape gets its name, is given in Exercise A10 to Chapter 10, p. 297 (there $\pi/t_a = b$, $a = \alpha b$). Applications of various Nyquist pulses can be found in J. G. Proakis and M. Salehi (2013).

Nyquist pulses $h$ allow the reconstruction of the values $x_k$ by sampling $s(t)$ even if $h$ and therefore $s$ are not bandlimited, thus despite aliasing effects in the spectrum of the pulse train $s_d(t) = \sum_{k=-\infty}^{+\infty} t_a s(kt_a)\delta(t - kt_a)$. In applications, $h$ is often a function with bounded support (see later p. 368). If the $x_k$ are referred to as symbols to be transmitted, then transmissions with Nyquist pulses are free from *inter-symbol interference* (abbreviated ISI in literature).

**Modulations with Pulse Shapes that are not Nyquist Pulses**

If we consider the task of reconstructing the values $x_k$ from the sampled values $s_k = s(kt_a)$, $k \in \mathbb{Z}$, of the received signal $s(t)$ as a discrete linear filter problem, then with the results on inverse discrete filters we obtain (see 11.6, p. 343 and 8.7, p. 181):

**Theorem 12.3.** *If a pulse shape $h$ corresponds to a discrete filter with impulse response $h_d = t_a \sum_{k\in\mathbb{Z}} h(kt_a)\delta_k$ that has an inverse with impulse response*

$h_{d,inv} = \sum_{k\in\mathbb{Z}} g_k\delta_k$, *so that* $(x_d * h_d) * h_{d,inv} = x_d * (h_d * h_{d,inv})$ *is associative* [9]*, then* $x_d = t_a \sum_{k\in\mathbb{Z}} x_k\delta_k$ *is reconstructed by the discrete convolution* $x_d = s_d * h_{d,inv}$*, i.e.*

$$x_n = \sum_{k\in\mathbb{Z}} s_k g_{n-k} \text{ for } n \in \mathbb{Z}.$$

Theorems on discrete filters in different signal spaces, on stability, causality, invertibility, and possible design methods for FIR or IIR filters were already presented in Section 11.6. Starting from the modulation of discrete information with various pulse shapes as impulse responses of linear filters, a variety of signal processing algorithms have been developed. Some aspects of this follow in Sections 12.5 on time-frequency analysis and 14.2 on wavelets. For an in-depth study of various methods of application-specific signal processing, reference is made here only to the extensive literature on the subject, for example, A. Papoulis (1977) on signal analysis, J. G. Proakis, M. Salehi (2013), L. W. Couch (2012) on digital communication systems, T. Salditt et.al. (2017) on imaging methods in biomedicine, or the works mentioned and referenced at the end of Section 12.1.

A study of digital signal processing, which today permeates almost every area of life and all fields of science, requires specialized training in dealing with the mathematical methods and ultimately with the technology through which designed algorithms can be implemented.

## 12.3 The Basic Idea of Multi-Carrier Transmission with OFDM

This section describes the basic idea of the OFDM multi-carrier method as a far-reaching technology. OFDM (English) stands for *Orthogonal Frequency Division Multiplexing*. Nearly everyone uses this method almost around the clock today, because OFDM is comprehensively used for the transmission of WLAN, DSL, digital radio (DAB) and TV (DVB), in powerline communication and mobile communication with LTE, LTE+, and 5G standards. An OFDM application in optical transmission systems with bandwidths up to 1 Tb/s is in development (see, for example, Y. Ma et al. (2010)). The history of Frequency Division Multiplexing (FDM), back then with analog technology, goes back to the first patents on multi-tone telegraphy in the years 1875-1876 by Alexander Graham Bell, Elisha Gray, and Thomas Edison. A readable account of the development of OFDM methods can be found in S. Weinstein (2009).

Today's digital OFDM methods, referred to as DMT (*Discrete Multitone Transmission*) in ADSL and VDSL, go back to works by R. Chang (1966) and S. Weinstein, P. Ebert (1971). They are a combination of applications of the DFT, the

[9] The $z$-transforms of $x_d$, $h_d$, $h_{d,\text{inv}}$ must have a common region of convergence.

sampling theorem with filter technology, together with the use of coding and encryption algorithms. Additionally, methods for estimating the properties of transmission channels are included, based on which transmission errors are to be corrected at the receiver to recover the user information. Physically, the OFDM methods are implemented with highly developed hardware in electrical and communications engineering.

Characteristic of OFDM transmission is that large parts of the required transmission and reception technology consist of discrete signal processing, which can be cost-effectively realized with uniquely developed algorithms on integrated circuits (ICs) compared to analog technology. Only because of this, today one can get a WLAN USB stick or digital media devices including necessary software as mass products for relatively low costs.

In the literature on communications engineering, there are a number of easily searchable textbooks dedicated in detail to the OFDM methods. Therefore, only the essential ideas will be presented here in all necessary brevity, as far as they can be easily understood with the methods of Fourier analysis treated in the present text. They may serve as an incentive for readers to deepen their knowledge with specialized literature if interested.

## Mathematical Components of an OFDM Transmission System

1. *From the Coded Bit Stream with QAM to Trigonometric Polynomials*
   On the sender side, there is a bit stream, i.e., a $01$ sequence of data that is to be transmitted. The data is usually encoded and encrypted (keywords: error-correcting codes, interleaving, possibly WPA2 encryption, etc.).
   To explain OFDM at hand of an example, let us assume that transmission is to be done with 16-QAM modulation. 16-QAM stands for *Quadrature Amplitude Modulation* with an alphabet of 16 complex numbers. From the bit stream, blocks of 4 bits each are injectively mapped to a set of 16 complex numbers, also referred to as QAM symbols (see Fig. 12.6).
   A 16-QAM modulation with its assignments is shown below. All complex values are multiplied by the scaling factor $A = 1/\sqrt{10}$. This normalizes the power of a 16-QAM modulated uniformly distributed $01$ random bit sequence in the transmit signal to one (cf. L. W. Couch (2012)).

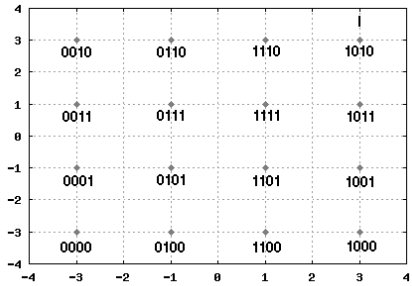


On the left is a mapping of 4 bits each with a Gray code to numbers in the complex plane (abscissa: real part, ordinate: imaginary part). For a further example, we set four 16-QAM mappings:

$1110 \to c_1 = A(1+3j)$
$1011 \to c_2 = A(3+j)$
$0010 \to c_3 = A(-3+3j)$
$0101 \to c_4 = A(-1-j)$

**Fig. 12.6.** 16-QAM Gray Coded Symbol Mapping without Factor $A$

To generate an OFDM symbol $S_i$ with $N$ carriers for a time period from $iT$ to $(i+1)T$, the sequential bit stream is parallelized into $n \leqslant N$ 4-bit blocks, which are mapped with 16-QAM to $n$ complex numbers $c_{i,k}$ as shown above.
With the $N$ carriers $\mathrm{e}^{j2\pi kt/T}$ and the complex amplitudes $c_{i,k}$, a trigonometric polynomial with a bandwidth $B \leqslant (N-1)/T$ Hz is formed, which is limited in duration to the interval $[iT,(i+1)T]$ by multiplication with a time window $Tg_{i,T}(t) = Tg_T(t-iT)$, resulting in the *OFDM symbol $S_i$ in the baseband*:

$$S_i(t) = T \sum_{k=0}^{N-1} c_{i,k}\, \mathrm{e}^{j2\pi kt/T}\, g_{i,T}(t).$$

$N-n$ carriers, whose frequencies are agreed upon between the transmitter and receiver, remain unoccupied with $c_{i,k} = 0$, or they can be used with predetermined amplitudes as *pilot carriers* or – prefixed to the symbol – as *preambles* at the receiver for channel estimation and synchronization (cf. also Example 4, p. 85). The useful information of $4n$ bits is thus contained in the assigned complex amplitudes $c_{i,k}$ of $S_i$. The function $g_T$ is the impulse response of the transmit filter.
We initially assume a rectangular window for $g_{i,T}$ to illustrate the basic idea of OFDM and consider only a single time step with $i = 0$. To simplify notation, the index $i$ is therefore omitted, and $Tg_{i,T} = w_T = 1_{[0,T[}$ is set ($w_T$ thus being the indicator function of the interval $[0,T[$). The trigonometric polynomial component in the OFDM symbol $S$ occupies the frequency band $[0,(N-1)/T]$. However, the product with a time window $w_T$ is no longer bandlimited, i.e., the spectrum of $S$ results in out-of-band interference. In implementations, one would therefore choose other windows $w_T$ whose amplitude spectrum falls off faster than that of a rectangular window.
The functions $\mathrm{e}^{j2\pi kt/T}\, w_T(t)$, $k = 0,\ldots,N-1$, form an orthogonal system in the space $L^2([0,T])$, the frequency band $[0,(N-1)/T]$ is divided by the carrier frequencies with fixed frequency spacing $1/T$, and all QAM values are transmitted together during the symbol duration $T$. Because of these properties, the method is called *Orthogonal Frequency Division Multiplexing*, abbreviated OFDM. Due to the orthogonality of the carriers, transmission interference at one of the carrier frequencies has no effect on the other carriers, i.e., there is no *inter-carrier interference* (ICI) – at least as long as the transmission channel does not cause frequency disper-

sion due to Doppler effects in moving receivers as in mobile communications, and it is neglected that a signal, which is not bandlimited due to the rectangular window $w_T$, is transmitted over a bandlimited channel. Distortions of a linear time-invariant channel, for example, due to multipath propagation and superpositions of multiple delayed signal sections arriving at the receiver, can be corrected there - with moderate noise - by estimating the channel impulse response.

The following Fig. 12.7 shows the magnitude spectra of $c_k\,\mathrm{e}^{j2\pi kt/T}\,w_T(t)$ for $k=1$ and $k=4$. It can be seen that the spectra are Nyquist pulses in the frequency domain (cf. p. 364), i.e., $|c_k\widehat{w}_T(\omega-2\pi k/T)|=0$ at each maximum point $\omega$ of the magnitude spectra $|c_n\widehat{w}_T(\omega-2\pi n/T)|$ for $n\neq k$ $(0\leqslant k,\,n\leqslant N-1)$. Fig. 12.8 shows in advance the shape of a typical WLAN spectrum, with $48$ data carriers and here for visibility exaggeratedly large $4$ pilot carriers. A transmission with a rectangle time window had the blue spectrum. Transmission with a common raised cosine window, explained a little later, has much less out-of-band emission, as is seen in the red spectrum.

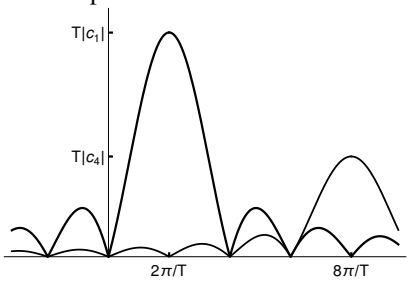


**Fig. 12.7.** Magnitude of two carriers

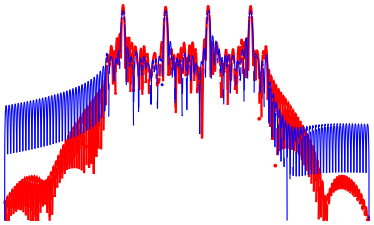

**Fig. 12.8.** Illustratively a WLAN spectrum

2. *Real-Valued Transmission Signal, Quadrature Modulation, and Demodulation*
A real transmission signal is obtained from $S$ through quadrature modulation (QM) with an intermediate frequency $\omega_c$. The generated real-valued signal $S_{\mathbb{R}}$ is

$$S_{\mathbb{R}}(t)=\Re\left(\mathrm{e}^{j\omega_c t}\sum_{k=0}^{N-1}c_k\,\mathrm{e}^{j2\pi kt/T}\right)w_T(t).$$

We obtain the following representation, where $I(t)$ is called the *in-phase* and $Q(t)$ the *quadrature component* of $S(t)$:

$$\begin{aligned}S_{\mathbb{R}}(t)&=\cos(\omega_c t)\sum_{k=0}^{N-1}\left(\Re(c_k)\cos(2\pi kt/T)-\Im(c_k)\sin(2\pi kt/T)\right)w_T(t)\\&\quad-\sin(\omega_c t)\sum_{k=0}^{N-1}\left(\Re(c_k)\sin(2\pi kt/T)+\Im(c_k)\cos(2\pi kt/T)\right)w_T(t)\\&=\left(I(t)\cos(\omega_c t)-Q(t)\sin(\omega_c t)\right)w_T(t).\end{aligned}$$

Pairwise orthogonality of the carriers and signal bandwidth are preserved in QM. The signal spectrum is shifted to the intermediate frequency $f_c=\omega_c/(2\pi)$ (for

WLAN, $f_c$ is about 2.4 GHz or 5 GHz). Repeated QM and low-pass filtering to suppress high-frequency remnants at the receiver return the complex-valued function $S$ in the baseband, assuming no influences from the transmission channel distort the signal. Using addition theorems for cosine and sine functions, we find

$$\begin{aligned} 2\cos(\omega_c t)S_{\mathbb{R}}(t) &= I(t) + \text{high-frequency remnant} \\ 2\sin(\omega_c t)S_{\mathbb{R}}(t) &= Q(t) + \text{high-frequency remnant} \\ S(t) &= I(t) + jQ(t). \end{aligned}$$

From samples of $S$, the receiver can then use a DFT to reconstruct the amplitudes $c_k$ and with inversion of the 16-QAM mapping, finally reconstruct the transmitted bit groups. In the following, it will be explained how to transition from this analog model with discrete signal processing to the digital transmission methods used today, saving much expensive analog technology.

3. *Use of Discrete Signal Processing with an IDFT*
To generate a transmission signal with discrete signal processing, samples of $S$ are generated from the amplitudes $c_k$ of the OFDM symbol with $M \geqslant N$ values. To demonstrate, we choose $M = 8$. An IDFT (see Section 6) of the amplitudes $c_0, \ldots, c_{M-1}$ suffices for this purpose without extensive hardware. For "upsampling" to $M$ values, a zero sequence of length $M - N$ is simply appended to the amplitudes $c_k$. The subsequent IDFT has length $M$ and provides $M$ samples $(y_n)_{0 \leqslant n \leqslant M-1}$. For radix-2 IFFT/FFT algorithms used in practice, $M$ is a power of two, such as $M = 2048$ for LTE with 20 MHz bandwidth, 1201 used carriers per OFDM symbol, 15 kHz carrier spacing, and 30.72 MHz sampling frequency.
With sufficient samples, potentially after further "upsampling" the IDFT values with *CIC filters* (Cascade Integrator Comb Filter), quadrature modulation can also be performed discretely without analog mixers by multiplying the real and imaginary parts of the IDFT list with the values of the modulating cosine and sine functions at the corresponding sample points and subtracting the resulting lists point by point. For that, one can use DDS components (Direct Digital Synthesizer) matching the bandwidth and bit resolution of the subsequent D/A converter. The result is samples of the real transmission signal $S_{\mathbb{R}}$, which are fed to a D/A conversion (see p. 359-361).

**Example.** With the data $T = 1/2$ s, $c_0 = 0, c_1, \ldots c_4$ as on p. 367, $M = 64$, $\omega_c = 64\pi$ rad/s, the following graph shows in Fig. 12.9 the QM modulation of the analog signal $S(t)$ (thin line) and the approximation (thick line), which is generated from IDFT values and discrete QM modulation as described. The second curve is drawn with a value offset of +0.4 for visible distinction. Fig. 12.10 shows the amplitude spectrum of the first curve in dB. For both cases, the *rectangular time window* $w = 1_{[0,T[}$ was used, and for interpolation of the samples in the second case, the series from the Shannon sampling theorem with bandwidth $B = 128\pi$ rad/s. The moderate roll-off of the amplitude spectrum, which does not meet practical requirements for permissible out-of-band emissions, is apparent

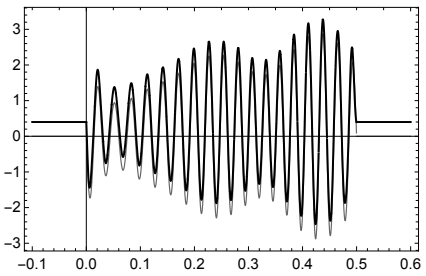


**Fig. 12.9.** QM-modulated signals over time $t$, analog signal and approximation from samples (thick) with offset

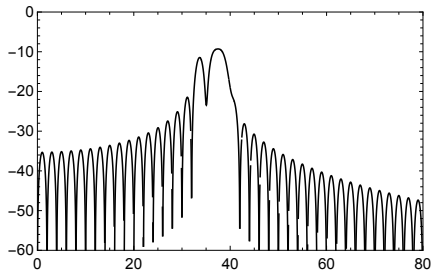


**Fig. 12.10.** Amplitude spectrum in dB, plotted over frequency $\omega_c/(2\pi) = 32$ Hz

4. *Other Pulse Shapes Reducing Out-of-Band Emissions, Cyclic Prefix and Postfix*
In practice, stronger damping in the out-of-band region is required. Specifications for WLAN, DAB, etc., define spectral masks that must be adhered to for transmission.
There are various methods to achieve better damping in the out-of-band region. One can quickly find a large number of publications on this topic under keywords like "OFDM Pulse Shaping". Methods such as smoothed time windows (W-OFDM for Windowed OFDM), filter banks for pulse shaping (FBMC, "Filter Bank Based Multicarrier Systems"), and other variants of the multicarrier method can be used. Important aspects are the Heisenberg's uncertainty principle and the Balian-Low theorem regarding the time-frequency localization of signals (see the following sections of this chapter).
In the following example, it is shown how the signal spectrum in the out-of-band region can be attenuated by extending the signal duration $T$ and using a time window $w_{T(1+\alpha)}$ of duration $T(1+\alpha)$ with rounded edges instead of the previously used rectangular window. At the same time, a "Cyclic Prefix" (CP) and a "Postfix" are introduced by cyclically extending the signal. While $\widehat{w}_T$ is a Nyquist pulse in the frequency domain, this is not the case for $\widehat{w}_{T(1+\alpha)}$. As a result, the transmit signal experiences some inter-carrier interference (ICI) because the carriers $\mathrm{e}^{j2\pi kt/T}\, w_{T(1+\alpha)}(t)$, $k = 0, \ldots, N-1$, are no longer orthogonal to each other. This method is, on the other hand, easy to implement and is also used in real systems (cf. L. Montreuil et al. (2013), Broadcom Recommendations for Tx Symbol Shaping).
An important advantage of the cyclic prefix is that the convolution with the channel impulse response $h$ of a time-invariant transmission channel can be represented as a cyclic convolution if this impulse response does not last longer than the prefix. This allows for interference suppression using the sample values $\widehat{h}(2\pi k/T)$ of the estimated channel frequency response $\widehat{h}$. More on this below in point 7. The time interval with the cyclic prefix is called the *Guard Interval* (GI). It often comprises $1/4$ of the core symbol duration (e.g., LTE[10]).

[10] LTE 4G with 64-QAM, 20 MHz bandwidth: 1201 subcarriers, core symbol $T = 66.67\,\mu$s, GI (long) $16.67\,\mu$s.

*Pulse shaping with "Raised Cosine Window", Cyclic Prefix, and Postfix*
The IDFT values from the previous example are now cyclically extended by a prefix with the last 16 IDFT samples and a postfix with the first 4 IDFT samples. The new list then has $L = 84$ elements. Instead of the rectangular time window, a window with cosine edges ("*raised cosine window*") is used as in the previously cited Broadcom recommendations[11]. Additionally, a realizable (analog) Butterworth low-pass filter is used for interpolating the samples of $S_{\mathbb{R}}$ instead of the Shannon sampling series to model the D/A conversion. For the weighting of the IDFT list with time window values, the time window $w_{T(1+\alpha)}(t) = Tp(t)$ is used with $\alpha = T/16$ and

$$p(t) = \begin{cases} 1/T & \text{for } 0 \leqslant |t| < \dfrac{T(1-\alpha)}{2} \\ \dfrac{1}{2T}\left(1+\cos\left(\dfrac{\pi}{\alpha T}\left(|t|-\dfrac{T(1-\alpha)}{2}\right)\right)\right) & \text{for } \dfrac{T(1-\alpha)}{2} \leqslant |t| \leqslant \dfrac{T(1+\alpha)}{2} \\ 0 & \text{otherwise.} \end{cases}$$

Weighting the cyclically extended IDFT list with values of $Tp\left(t - \dfrac{T(1+\alpha)}{2}\right)$ at times $t_n = T(1+\alpha)(2n+1)/(2L)$, $n = 0, \ldots L-1$, results in the first 3 prefix values and the last 3 postfix values entering the cosine edges of the window, thus "rounding" the OFDM pulse shape. Below on the left is the interpolated signal with low-pass delay and cyclic extensions at the beginning and end, and on the right, the resulting amplitude spectrum is shown in bold compared to the thinly drawn one using the rectangular window. (Try to examine the example yourself with a computer algebra system.) See also the figure on p. 368.
From the Fourier transform $\widehat{p}$ (cf. Exercise A10, p. 297), it can be seen that the amplitude spectrum of the OFDM signal in the out-of-band region is now much more attenuated than with the rectangular window, as can also be clearly seen in the following Fig. 12.12:

$$\widehat{p}(\omega) = \frac{\sin(\omega T/2)}{\omega T/2}\left(\frac{\cos(\alpha\omega T/2)}{1-(\alpha\omega T/\pi)^2}\right).$$

The Butterworth filter for interpolation was designed with the following data: passband edge 48 Hz, stopband edge 96 Hz, minimum passband gain 0.9, maximum stopband gain 0.005, DC gain $K = 1$ (Fig. 12.11). The order of the filter is 9, the group delay approximately 21 ms in the passband (cf. p. 312). The attenuation gain in the range up to the intermediate frequency is due to the Raised Cosine Window, the even stronger fall-off of the spectrum in the right part of the last image is due to the additional attenuation in the stopband of the low-pass filter.

[11] Broadcom is a supplier, e.g., for DSL in wired connections (DSLAMs) of various providers.

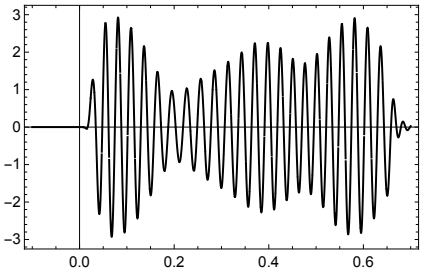


**Fig. 12.11.** QM-modulated signal with the raised cosine window over time $t$ in seconds, after interpolation with Butterworth low-pass filter, group delay in the passband $\sim$ 21 ms; signal extended by pre- and postfix

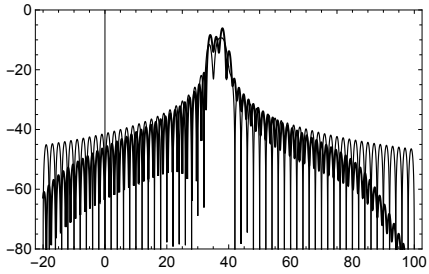


**Fig. 12.12.** dB amplitude spectra over frequency $f$ ($f_c = \omega_c/(2\pi) = 32$ Hz), bold with raised cosine window, thin with rectangular window. For $f < f_c$ window effect, beyond the stopband edge 96 Hz, additional low-pass effect

5. *Reconstruction of the Information with a DFT for Identical Reception of $S_{\mathbb{R}}$*
With identical reception without distortions caused by the transmission channel, the receiver retrieves the in-phase component $I(t)$ and the quadrature component $Q(t)$ of the signal by extracting a time interval of duration $T$ and inverting the quadrature modulation. After an $N$-point DFT of $I(t) + jQ(t)$ over this time interval, it can be determined which complex amplitudes $c_k$ of the OFDM alphabet correspond to the DFT result. One primary advantage of periodicity with prefix and postfix is that moderate synchronization errors (phase offset) can be easily corrected if pilot values among the amplitudes are known.

**Example.** Sampling in the previously calculated example[12] with sampling times $t_n = nT/N + \Delta t$, $N = 5$, $n = 0, \ldots, N-1$ and $\Delta t = 0.226$ s, i.e., asynchronously starting in the prefix, initially yields the DFT list dft

$$\begin{aligned}\text{dft} = (\ &-0.00136 + 0.00096j, -2.10649 + 2.35922j, -2.37870 + 2.08454j,\\ &+3.02492 - 2.97252j, -0.37881 + 1.36073j).\end{aligned}$$

Using $c_1$ as a pilot value results in the corrected phase (cf. Example 4, p. 85) giving the result $(\widetilde{c}_0, \ldots, \widetilde{c}_4)$, which can now be compared with the values $(c_0, \ldots, c_4)$ on p. 367. The deviations between the two lists are due to rounding during the discrete Fourier transforms and slight inter-carrier interferences caused by the window $w_{T(1+\alpha)}$:

$$\begin{aligned}\frac{1}{A}(\widetilde{c}_0, \ldots, \widetilde{c}_4) &= (-0.0013644 + 0.00095966j,\ 1.00016 + 3.00049j,\\ &\quad 3.0015 + 0.997246j,\ -2.99428 + 3.00339j,\ -1.00272 - 0.994806j)\\ \frac{1}{A}(c_0, \ldots, c_4) &= (\,0,\ 1 + 3j,\ 3 + 1j,\ -3 + 3j,\ -1 - 1j\,).\end{aligned}$$

[12] Recommendation: Compute the example yourself using a computer algebra system.

6. *Energy Density and Spectral Power Density of an OFDM Transmission*
An OFDM transmission, like the segment under consideration, is time-limited and thus an energy signal. Therefore, there is no power density in the usual sense other than zero. The squared magnitude of $\widehat{S_{\mathbb{R}}}(\omega)$ in the example represents an energy density according to its physical dimension. The spectrum of the approximation for $S_{\mathbb{R}}$ is, as seen in the example, essentially determined by the variance of the OFDM alphabet and the Fourier transforms of the window function and the interpolating low-pass filter. In theoretical approaches, an OFDM transmission can be modeled as an infinitely lasting cyclostationary stochastic process, and an average spectral power density can be specified. Calculations under various assumptions about the modulation method can be found in L. W. Couch (2012) or W. A. Gardner, A. Napolitano, L. Paura (2008). The specifications of the transmission methods (WLAN, DVB-T, etc.) provide *spectral masks for spectral power densities* that must be adhered to – for signals in volts, then with the unit $\mathrm{V}^2$/Hz. In practice, this evidence is provided through simulations for spectral estimation. For this purpose, several thousand OFDM symbols are generated with a random bit sequence, and the interpolation of the (discrete) DFT spectra is averaged for spectral estimation. Various averaging methods are in use (averaged periodogram technique, Bartlett's method, Welch's method, etc.). A comprehensive treatment of the topic *spectral estimation* with statements on consistency, unbiasedness, and variance of various estimates can be found, for example, in the textbook on digital signal processing by K. D. Kammeyer, K. Kroschel (2012).

7. *Effects of the Transmission Channel, Preambles, Pilots, and Cyclic Prefix*
The transmission channel for OFDM, whether wired or wireless, has various effects on the functionality and quality of the transmission. These are summarized under the term "fading". These include echo effects and time delays in multipath propagation, leading to possible cancellations or intersymbol interference (ISI), attenuation for various reasons (transmitter distance, weather), frequency dispersion due to Doppler effects with moving transmitters or receivers. Additionally, noise, nonlinear distortions of the RF amplifiers, especially in mass products designed with cost and energy optimizations, jitter effects in oscillators in components, and much more, which communications engineers must master for a robust functioning overall system during design and implementation. An initial impression of the topic of channel equalization is given by the following considerations:
Assume that the receiver has the sampled values $r(nT/N)$ $(0 \leqslant n \leqslant N-1)$ of the received signal segment. The channel is assumed to be a noiseless causal linear filter. Its impulse response $h$ should decay within the duration of a cyclic prefix preceding the OFDM symbol. Through the extension of the symbol with prefix and postfix as in the example and the decay of transient components of the convolution of the signal $S$ with $h$ within the prefix duration, the values $r(nT/N)$ can be regarded as sampled values of the convolution of $h$ with the $T$-periodic Fourier series $S_T$, which arises through the periodicity of the OFDM symbol. Since $\mathrm{supp}(h)$ is bounded, $\widehat{h}$ is a multiplier in $\mathcal{S}'$. With sampled values of the channel frequency response $\widehat{h}$, the periodized received signal $r_T$ satisfies (cf. p. 279 and p. 321):

$$r_T(t) = S_T * h = \sum_{k=0}^{N-1} c_k \widehat{h}(2\pi k/T)\, \mathrm{e}^{j2\pi kt/T}\,.$$

It follows that $r(nT/N) = r_T(nT/N) = \sum_{k=0}^{N-1} c_k \widehat{h}(2\pi k/T)\, \mathrm{e}^{j2\pi kn/N}$, i.e., $r(nT/N)$ is the $n$-th component of an IDFT of $\left(c_k \widehat{h}(2\pi k/T)\right)_{k=0,\ldots,N-1}$.
A DFT of the values $r(nT/N)$ with result $\widehat{r}_k$ ($0 \leqslant k \leqslant N-1$) in the $k$-th component then shows for a desired complex amplitude $c_k$ of the OFDM symbol:

$$c_k = \frac{\widehat{r}_k}{\widehat{h}(2\pi k/T)}.$$

Preambles and pilot symbols known to the receiver can be used for synchronization and for estimating the impulse response $h$ or the channel frequency response $\widehat{h}$. However, this seemingly simple channel equalization must be approached with caution. The necessary duration of the prefix and the channel frequency response $\widehat{h}$ must be reliably estimated; the values $\widehat{h}(2\pi k/T)$ must not become zero (cf. Sections 5.6 and 11.6 on convolution inverses), and the convolution equation $r = S * h$ is a typical ill-posed problem (cf. Excercise A12 in Chapter 9). Very small values of $\widehat{h}(2\pi k/T)$ in the quotient for $c_k$ cause a strong increase in noise components in the received signal that were not considered. Therefore, in real practice, there are various modified equalization algorithms, with known $\widehat{h}$ – for example, in wired transmissions – partially with pre-equalization already at the transmitter, otherwise at the receiver side.

8. *Final Remarks and Notes on Advanced Communication Technology*
There are many other topics that need to be mastered for practical real-time transmission (within a few $\mu$s per OFDM symbol, see footnote[11]) with OFDM or modifications of the procedure (OFDMA, COFDM, FBMC, GFDM, etc.). These include, in particular, peak reduction (with many equal amplitudes $c_k$ in the OFDM symbol, *peak-to-average power ratio reduction, PAPR reduction*), channel equalization with multiple frequency-selective channels (Doppler effects with moving transmitters or receivers with frequency dispersion), and many others. Despite simple principles, it is a long way to robust technology, demanding high skill from engineers and computer scientists. Since this text can by no means be a comprehensive introduction to the art of communication technology, but only aims to describe some fundamental ideas originating in Fourier analysis and essentially provide suggestions for acquiring further knowledge on the subject if interested, the already frequently cited specialized literature on communication technology is recommended once again for everything else mentioned in the text.

## 12.4 Heisenberg's Uncertainty Principle

Already in earlier sections, we had qualitatively observed that the spectral width of a signal is greater the shorter the signal duration is. Conversely, the impulse response of a low-pass filter lasts perceptibly longer in time the smaller the cut-off frequency of the filter is. The same aspect shows up in the scaling property $f(\alpha t) \multimap\!\bullet \frac{1}{|\alpha|}\widehat{f}\left(\frac{\omega}{\alpha}\right)$ of the Fourier transform for $\alpha \neq 0$ or in the fact that a time-limited signal $f$ has a Fourier transform $\widehat{f}$ that does not completely vanish in any frequency interval (see p.281). For illustration, one can look again at the examples in Sections 10.1 and 11.2, such as rectangular or triangular functions with their Fourier transforms on p.254 or the correspondences $\delta(t) \multimap\!\bullet 1$ and $1 \multimap\!\bullet 2\pi\delta(\omega)$.

To obtain quantitative statements about the observed coupling of compression and expansion in the time-frequency domain, a measure is needed for the duration and bandwidth of signals. Although there is no uniform definition of duration and bandwidth for the immense variety of possible signals, the definition of dispersion is suitable for introducing these concepts for a large class of signals. For the signals $f$ considered below, we assume that the functions $f$ are continuous and piecewise continuously differentiable. Furthermore, $tf(t)$ and $\dot{f}(t)$ should also be square-integrable along with $f(t)$. We interpret the parameter $t$ as a time parameter.

**Definition.** 1. *The dispersion $\Delta_a^2(f)$ of $f \neq 0$ around the point $a$ is defined by*

$$\Delta_a^2(f) = \frac{\int\limits_{-\infty}^{+\infty} (t-a)^2 |f(t)|^2 \,\mathrm{d}t}{\int\limits_{-\infty}^{+\infty} |f(t)|^2 \,\mathrm{d}t}.$$

2. *The effective duration $D_t(f)$ of $f \neq 0$ is defined by*

$$D_t(f) = \Delta_a(f) \quad \textit{with} \quad a = \frac{\int\limits_{-\infty}^{+\infty} t|f(t)|^2 \,\mathrm{d}t}{\int\limits_{-\infty}^{+\infty} |f(t)|^2 \,\mathrm{d}t}.$$

3. *The effective bandwidth $D_\omega(f)$ of $f \neq 0$ is defined by*

$$D_\omega(f) = \Delta_b(\widehat{f}) \quad \textit{with} \quad b = \frac{\int\limits_{-\infty}^{+\infty} \omega|\widehat{f}(\omega)|^2 \,\mathrm{d}\omega}{\int\limits_{-\infty}^{+\infty} |\widehat{f}(\omega)|^2 \,\mathrm{d}\omega}.$$

The dispersion $\Delta_a^2(f)$ is a measure of how well or poorly $f$ is "concentrated around $a$". If $|f(t)|$ is very small outside a small neighborhood of $a$, then the factor $(t-a)^2$ makes the numerator of $\Delta_a^2(f)$ small compared to the denominator, and the dispersion is small. If $|f(t)|$ is large for $(t-a)^2 > 1$, the same factor

causes an increase in the numerator compared to the denominator, and the dispersion becomes large. If we interpret the function $|f(t)|^2$ as mass density, then $S = \int_{-\infty}^{+\infty} t|f(t)|^2\,\mathrm{d}t \,/ \int_{-\infty}^{+\infty} |f(t)|^2\,\mathrm{d}t$ is the center of mass and $\Delta_S^2(f)$ is the moment of inertia with respect to the center of mass. If we interpret the function $|f(t)|^2 / \int_{-\infty}^{+\infty} |f(t)|^2\,\mathrm{d}t$ as the density of a probability distribution, then $S$ is the expected value and $\Delta_S^2(f)$ is the variance of the probability distribution.

## Examples

1. For $f(t) = (2\pi\sigma^2)^{-1/4}\,\mathrm{e}^{-(t-m)^2/(4\sigma^2)}$, $\sigma > 0$, the function $|f(t)|^2$ is the density of the Gaussian distribution known from probability theory with mean $m$ and variance $\sigma^2$. The effective duration of $f$ is therefore according to the previous remark $D_t(f) = \sigma$. Using *Plancherel's theorem* and the *differentiation rule* for the Fourier transform, the effective bandwidth follows:

$$D_\omega^2(f) = \Delta_0^2(\widehat{f}) = \frac{1}{2\pi}\int_{-\infty}^{+\infty} \omega^2|\widehat{f}(\omega)|^2\,\mathrm{d}\omega = \frac{1}{2\pi}\int_{-\infty}^{+\infty} |\widehat{\dot{f}}(\omega)|^2\,\mathrm{d}\omega$$
$$= \int_{-\infty}^{+\infty} |\dot{f}(t)|^2\,\mathrm{d}t = \frac{1}{4\sigma^4}\int_{-\infty}^{+\infty} (t-m)^2|f(t)|^2\,\mathrm{d}t = \frac{1}{4\sigma^2}.$$

   The product of effective duration and bandwidth yields $D_t(f)D_\omega(f) = \dfrac{1}{2}$.

2. For the triangular function $f(t) = \begin{cases} A(1-|t|/T) & \text{for } |t| \leqslant T \\ 0 & \text{for } |t| > T \end{cases}$, one calculates

$$\int_{-\infty}^{+\infty} |f(t)|^2\,\mathrm{d}t = \frac{2A^2T}{3} \quad \text{and the effective duration is} \quad D_t(f) = \frac{T}{\sqrt{10}}.$$

   According to Plancherel's theorem, $\displaystyle\int_{-\infty}^{+\infty} |\widehat{f}(\omega)|^2\,\mathrm{d}\omega = \frac{4\pi A^2 T}{3}$. The center of mass of $|\widehat{f}|^2$ is zero because $|\widehat{f}|^2$ is an even function. As in the first example, it follows that

$$\int_{-\infty}^{+\infty} \omega^2|\widehat{f}(\omega)|^2\,\mathrm{d}\omega = \int_{-\infty}^{+\infty} |\widehat{\dot{f}}(\omega)|^2\,\mathrm{d}\omega = 2\pi\int_{-\infty}^{+\infty} |\dot{f}(t)|^2\,\mathrm{d}t = \frac{4\pi A^2}{T}.$$

The effective bandwidth is thus $D_\omega(f) = \sqrt{3}/T$. The time-bandwidth product is

$$D_t(f)D_\omega(f) = \sqrt{3}/\sqrt{10} \approx 0.548,$$

i.e., about $9.6\%$ larger than in the first example with the Gaussian function.

**Illustratively.** The calculations in these examples show us that $\omega\widehat{f}(\omega)$ is square-integrable if and only if $\dot{f}(t)$ has this property. *Since the bandwidth is given by an integral over the squared magnitude of the derivative $\dot{f}$ of a time signal $f$, a compression of the signal $f$ must cause an increase in the bandwidth through simultaneously growing slopes.* Therefore, the functions $f$ and $\widehat{f}$ cannot be simultaneously concentrated near individual points. A quantitative description of this fact is provided by Heisenberg's uncertainty principle. It was discovered by W. Heisenberg in 1927 in quantum mechanics. Its significance for signal transmission was investigated by D. Gabor (1946) . In our context, it reads as follows:

## Uncertainty Principle for the Time-Bandwidth Product.

**Theorem 12.4** (Time-Bandwidth Product)**.** *For square-integrable signals $f \neq 0$ and any $a, b \in \mathbb{R}$ the following holds*

$$\Delta_a^2(f)\Delta_b^2(\widehat{f}) \geqslant \frac{1}{4}.$$

*In particular, for the time-bandwidth product, it always holds that $D_t(f)D_\omega(f) \geqslant \dfrac{1}{2}$. Equality $D_t(f)D_\omega(f) = 1/2$ holds if and only if $|f|$ is a Gaussian function, i.e., if $f(t) = c\,\mathrm{e}^{jat}\,\mathrm{e}^{-(t-m)^2/(4\sigma^2)}$ with any real constants $a$, $m$, $c \neq 0$, $\sigma \neq 0$.*

*Proof.* We can assume that with $f$, also $tf(t)$ and $\dot{f}(t)$ are square-integrable, otherwise $\Delta_a^2(f) = \infty$ or $\Delta_b^2(\widehat{f}) = \infty$ would hold and the inequality would be trivially satisfied. For $a = b = 0$, integration by parts yields

$$\int_\alpha^\beta \overline{tf(t)}\dot{f}(t)\,\mathrm{d}t = t|f(t)|^2\Big|_\alpha^\beta - \int_\alpha^\beta \Big(|f(t)|^2 + tf(t)\overline{\dot{f}(t)}\Big)\,\mathrm{d}t\,,$$

so

$$\int_\alpha^\beta |f(t)|^2\,\mathrm{d}t = -2\Re\Big(\int_\alpha^\beta \overline{tf(t)}\dot{f}(t)\,\mathrm{d}t\Big) + t|f(t)|^2\Big|_\alpha^\beta.$$

Due to the assumptions about $f$ (cf. p. 375), the limits of the integrals exist for $\alpha \to -\infty$, $\beta \to +\infty$ and it holds that $\lim\limits_{\alpha\to-\infty} \alpha|f(\alpha)|^2 = \lim\limits_{\beta\to+\infty} \beta|f(\beta)|^2 = 0$. Thus, it follows

$$\int_{-\infty}^{+\infty} |f(t)|^2 \,\mathrm{d}t = -2\Re\Big( \int_{-\infty}^{+\infty} \overline{tf(t)}\dot{f}(t) \,\mathrm{d}t \Big).$$

Using the Cauchy-Schwarz inequality and Plancherel's theorem we obtain

$$\begin{aligned}\Big( \int_{-\infty}^{+\infty} |f(t)|^2 \,\mathrm{d}t \Big)^2 &\leqslant 4\Big( \int_{-\infty}^{+\infty} t^2|f(t)|^2 \,\mathrm{d}t \Big)\Big( \int_{-\infty}^{+\infty} |\dot{f}(t)|^2 \,\mathrm{d}t \Big) \\ &= 4\Big( \int_{-\infty}^{+\infty} t^2|f(t)|^2 \,\mathrm{d}t \Big)\Big( \frac{1}{2\pi} \int_{-\infty}^{+\infty} \omega^2|\widehat{f}(\omega)|^2 \,\mathrm{d}\omega \Big)\end{aligned}$$

and hence the uncertainty relation $\Delta_0^2(f)\Delta_0^2(\widehat{f}) \geqslant \dfrac{1}{4}$.

The general case for $a \neq 0$ or $b \neq 0$ can be obtained with $g(t) = \mathrm{e}^{-jbt}\, f(t+a)$. Since $\Delta_a^2(f) = \Delta_0^2(g)$ and $\Delta_b^2(\widehat{f}) = \Delta_0^2(\widehat{g})$ hold, it follows

$$\Delta_a^2(f)\Delta_b^2(\widehat{f}) = \Delta_0^2(g)\Delta_0^2(\widehat{g}) \geqslant \frac{1}{4}.$$

The Cauchy-Schwarz inequality above becomes an equality if and only if $tf(t)$ and $\dot{f}(t)$ are linearly dependent, i.e., if the differential equation $ktf(t) = \dot{f}(t)$ holds (cf. p. 286). The only nontrivial, square-integrable solutions of this differential equation are of the form $f(t) = c\,\mathrm{e}^{kt^2/2}$ with $c \neq 0$, $k < 0$. With $k = -1/(2\sigma^2)$, the last statement of the theorem follows. □

**Remark.** The smoothness assumptions on $f$ from p. 375 can be omitted as with Plancherel's theorem (cf. p. 264), i.e., the Heisenberg uncertainty relation holds for any square-integrable functions $f$. A proof of this more general statement was given in 1931 by W. Pauli and H. Weyl. It can be found, for example, in the textbook of H. Dym and H. P. McKean (1985).

## Application Examples

1. *Resolution in the Time Domain.* In electrical measurement technology, it is known that, for example, with an oscilloscope of 100 MHz effective bandwidth ($D_\omega = 2\pi \cdot 100\,\mathrm{MHz}$), only a temporal resolution in the order of 1 ns is possible, with $D_\omega$ as above, $D_t \geqslant 1/(2D_\omega) \approx 0.8 \cdot 10^{-9}$ s. For signals of shorter effective duration, the oscilloscope acts as a low-pass filter, the signals are no longer exactly reproduced, but smoothed in reproduction and prolonged in duration. Start and stop pulses for measuring time intervals below the duration given by the uncertainty principle then merge in the reconstruction; a time measurement of such short intervals is therefore no longer possible.

2. *Resolution in the Frequency Domain.* The effective duration $D_t$ for which one must sing a tone or play an instrument to assign it a pitch or frequency with the accuracy $D_\omega$ is, according to the uncertainty principle, at least $1/(2D_\omega)$. For instance, if $D_\omega = 2\pi \cdot 1\,\text{Hz}$, then $D_t$ must be greater than about $8 \cdot 10^{-2}\,\text{s}$. In very fast passages of a musical piece, slight intonation weaknesses of the virtuosos cannot be noticed. Therefore, amateur musicians are recommended to choose the fastest possible musical pieces for a potential performance.
3. *Ultra-Short Pulse Laser of High Bandwidth.* The pulse duration of today's mode-locked short pulse lasers is in the range of a few femtoseconds (1 fs $= 10^{-15}$ s) with typical pulse repetition rates of 80-100 MHz up to 20-30 GHz. The corresponding enormous bandwidths enable time-resolved spectroscopy, for example in the analysis of chemical reactions. In terahertz time domain spectroscopy (THz-TDS), a non-invasive broadband method for investigating material properties in the far-infrared is available. Application areas include investigations of crystal structures, biomedical diagnostics, or pharmaceutical quality control. Readers interested in laser technology are referred to the textbook C. Rullière (1998).

## Heisenberg's Uncertainty Principle in Quantum Mechanics

Since the Copenhagen Conference in 1927, atomic physics has undergone a probabilistic interpretation with quantum mechanics. In this interpretation, experimental experiences, their theoretical description, and interpretation were brought together, unifying both the wave model and the particle model of matter without contradiction. Historical developments of quantum mechanics and its mathematical foundations can be found in works by P. A. M. Dirac (2008), A. Messiah (2003), or other relevant literature.

Heisenberg's uncertainty principle holds a central position in the development and interpretation of quantum theory. To formulate it in the language of quantum mechanics, we consider a free electron moving along the $x$-axis. However, its state at a fixed time cannot be specified by a position $x_0 \in \mathbb{R}$ and a momentum $p_0 \in \mathbb{R}$ as in classical mechanics, but is described by a complex-valued, square-integrable wave function $\psi(x)$, whose $L^2$ norm is

$$\|\psi\|_2 = \left( \int_{-\infty}^{+\infty} |\psi(x)|^2 \, \mathrm{d}x \right)^{1/2} = 1.$$

The functions $x\psi(x)$ and $\dot{\psi}(x)$ are also assumed to be square-integrable with $\psi(x)$. The function $|\psi|^2$ is interpreted as the probability density of the electron's presence. The position of the particle is thus a random variable with the expected value

$a = \int_{-\infty}^{+\infty} x|\psi(x)|^2 \,\mathrm{d}x$ and the variance $\Delta_a^2(\psi)$. The probability that a position measurement in the state $\psi$ yields a value $x \in [x_1, x_2]$ is $\int_{x_1}^{x_2} |\psi(x)|^2 \,\mathrm{d}x$.

The variance $\Delta_a^2(\psi)$ is a measure of the uncertainty of the position, as the larger the variance, the greater the probability of presence in intervals that do not contain the expected value $a$. If the variance is very small, then the position is said to be sharply determined. The probability of presence in very small intervals around $a$ is then large because the density function $|\psi|^2$ is concentrated around $a$ for small variance.

The momentum of the electron is essentially given by the Fourier transform of $\psi$, namely by the function

$$\widetilde{\psi}(p) = (2\pi\hbar)^{-1/2}\widehat{\psi}(p/\hbar)$$

The constant $\hbar$ is the reduced Planck constant. The momentum is also a random variable. The function $|\widetilde{\psi}|^2$ is interpreted as the probability density for the momentum distribution. The expected value $b$ for a momentum measurement is then

$$b = \int_{-\infty}^{+\infty} p|\widetilde{\psi}(p)|^2 \,\mathrm{d}p = \frac{\hbar}{2\pi}\int_{-\infty}^{+\infty} p|\widehat{\psi}(p)|^2 \,\mathrm{d}p\,.$$

The variance $\Delta_b^2(\widetilde{\psi})$ is a measure of the uncertainty of the particle's momentum. The sharper the momentum is determined, the smaller $\Delta_b^2(\widetilde{\psi})$ is. For the product of the variances of $\psi$ and $\widehat{\psi}$, the uncertainty relation $\Delta_a^2(\psi)\Delta_{b/\hbar}^2(\widehat{\psi}) \geqslant 1/4$ holds according to p. 377. From

$$\begin{aligned}\Delta_b^2(\widetilde{\psi}) &= \frac{1}{2\pi\hbar}\int_{-\infty}^{+\infty}(p-b)^2\left|\widehat{\psi}\left(\frac{p}{\hbar}\right)\right|^2 \mathrm{d}p \\ &= \frac{\hbar^2}{2\pi}\int_{-\infty}^{+\infty}\left(p-\frac{b}{\hbar}\right)^2|\widehat{\psi}(p)|^2\,\mathrm{d}p = \hbar^2\Delta_{b/\hbar}^2(\widehat{\psi})\end{aligned}$$

the following uncertainty principle, discovered by W. Heisenberg (1901-1976) in 1927, results. It is one of the fundamental statements of quantum mechanics.

**Heisenberg's Uncertainty Principle.** *Position and momentum of an electron in the state $\psi$ are not simultaneously sharply defined, but rather afflicted with an uncertainty. For the wave functions $\psi$ and $\widetilde{\psi}$, the following uncertainty relation holds*

$$\Delta_a(\psi)\Delta_b(\widetilde{\psi}) \geqslant \hbar/2.$$

The statement also applies to wave functions in three-dimensional space. One just needs to apply the Fourier transform for functions of several variables. The uncertainty relation is *not* based on limits of measurement accuracy, but is a *general property of functions*. For example, one can speak of the frequency of an oscillation "in the pure sense" only if the oscillation process is periodic and thus particularly unlimited in time. A duration is then entirely undefined. Conversely, the shorter the process lasts, the more questionable it is to speak of periodicity and thus of frequency; the concept itself becomes fuzzy, the process must be mathematically described by the corresponding spectral function instead of a pure frequency, and uncertainty relations arise. In electrical engineering, this fact is known, as we have seen, in the case of the time duration-bandwidth product. Quantum mechanics shows that even position and momentum in the physical description of atomic particles through probability densities are subject to such uncertainties. The same applies to other quantities whose product yields an action. For example, one obtains an analogous uncertainty relation for the product of energy and duration of an atomic event. Applications of the uncertainty principle to questions in physics, such as the explanation of the tunneling effect, can be found in according literature.

## 12.5 Time-Frequency Analysis, Windowed Fourier Transforms

For many applications in signal processing, the Fourier transform in its original form is not suitable. Because the Fourier integral extends over the entire time axis, a full knowledge of the signal's time course would be necessary to analyze the spectral properties of a signal, including knowledge of all future signal values $t > t_0$ for analysis at a fixed time $t_0$. Furthermore, the asymptotic properties of the Fourier transform show that even temporally narrow disturbances affect the entire spectrum (see p. 262). In its classical form, the Fourier transform also does not allow for simultaneous time-frequency analysis. For example, speech or a piece of music in our everyday experience has a specific "time pattern" and at the same time a specific "frequency pattern". However, the spectral function of a signal does not show at what times and with what respective amplitudes a specific angular frequency $\omega$ occurs in a signal $f$, but rather accumulates contributions of the same angular frequency $\omega$ over the entire time course of $f$ in $\widehat{f}(\omega)$. D. Gabor (1900-1979) already noticed these disadvantages for signal processing purposes, and in 1946 in his work "Theory of Communication," he proposed time-frequency localization through Fourier transforms with window functions.

To obtain information about the "time-frequency pattern" of a signal, one determines not the spectral function $\widehat{f}$ of the entire signal, but the spectral functions for time segments of $f$. Time segments of a signal $f$ are obtained by multiplying $f$ with functions of finite effective duration. Such functions are referred to as window functions or time windows.

## Windowed Fourier Transforms, Gabor Transform

All signals $f$ and window functions $w$ are assumed to be piecewise continuously differentiable and square-integrable. For a window functions $w$, we assume that $w \neq 0$ and furthermore that with $w(t)$ and $\widehat{w}(\omega)$, both $tw(t)$ and $\omega\widehat{w}(\omega)$ are also square-integrable. The window functions $w$ then have finite effective duration and bandwidth (see 12.4). In particular, $|t|^{1/2}w(t)$ and $(1+|t|)w(t)$ are square-integrable, and the Cauchy-Schwarz inequality for the product $(1+|t|)^{-1}(1+|t|)w(t)$ shows that $w(t)$ is integrable.

Analogously, $\widehat{w}(\omega)$ is integrable. The functions $w(t)$ and $\widehat{w}(\omega)$ are then also continuous. As in previous sections (see p. 290), we use the notations $\langle f(t)|g(t)\rangle = \int_{-\infty}^{+\infty} f(t)\overline{g(t)}\,\mathrm{d}t$ for the inner product of square-integrable functions and $\|f\| = \langle f(t)|f(t)\rangle^{1/2}$ for the norm of $f$ in $L^2(\mathbb{R})$. The quantities

$$t^* = \langle tw(t)|w(t)\rangle/\|w\|^2 \;\text{ or }\; \omega^* = \langle \omega\widehat{w}(\omega)|\widehat{w}(\omega)\rangle/\|\widehat{w}\|^2$$

are referred to as the *time center* and *frequency center* of a window $w \neq 0$ (see p. 376).

**Definition.** *The transform $\mathcal{G}_w$, which maps a signal $f$ to the function $\mathcal{G}_w f = \widetilde{f}$, defined by* $\widetilde{f}(\omega,t) = \langle f(s)|w(s-t)\,\mathrm{e}^{j\omega s}\rangle = \int_{-\infty}^{+\infty} f(s)\overline{w(s-t)}\,\mathrm{e}^{-j\omega s}\,\mathrm{d}s$, *is called the windowed Fourier transform with the time window $w$. It is also abbreviated as STFT (Short Time Fourier Transform). The windowed Fourier transform with the Gaussian window $w(t) = g_\alpha(t) = (4\pi\alpha)^{-1/2}\,\mathrm{e}^{-t^2/(4\alpha)}$, $\alpha > 0$, is referred to as the Gabor transform $\mathcal{G}_\alpha$.*

Instead of periodic harmonic oscillations $\mathrm{e}^{j\omega t}$, the windowed Fourier transform uses translations of amplitude-modulated oscillations with the envelope $w$. To give an illustrative interpretation of $\widetilde{f}(\omega_0,t_0)$ for fixed $\omega_0$ and $t_0$, consider the first two bars[13] of the wonderful flute piece "Syrinx"of Claude Debussy (1862-1918):

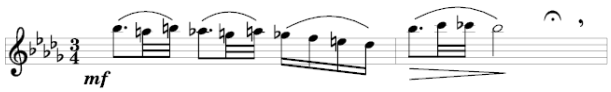


**Fig. 12.13.** From "Syrinx"of Claude Debussy

The "time-frequency pattern" is given in musical notation by the positions and note values of the individual notes, supplemented by dynamic indications such as "forte" or "piano". Similarly, one can consider the function

[13] The invention of musical notation is - like others - an ingenious human achievement and its expressive possibilities are inexhaustible.

$$w_{\omega_0,t_0}(s) = w(s - t_0)\,\mathrm{e}^{j\omega_0 s}$$

for a time window $w$ with the time center $t^*$ and the frequency center $\omega^*$ as a "note", which is localized in the frequency range around $\omega_0 + \omega^*$ with the effective bandwidth $D_\omega(w)$ and in the time range around $t_0 + t^*$ with the effective duration $D_t(w)$ (Fig. 12.14).

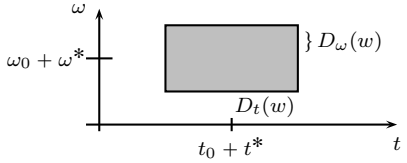


**Fig. 12.14.** Time-frequency localization of the "note" $w_{\omega_0,t_0}$ in the time-frequency window $[t_0 + t^* - D_t(w), t_0 + t^* + D_t(w)] \times [\omega_0 + \omega^* - D_\omega(w), \omega_0 + \omega^* + D_\omega(w)]$

The complex number $\widetilde{f}(\omega_0, t_0) = \langle f(s)|w_{\omega_0,t_0}(s)\rangle$ then indicates (see p. 54), the extent to which the "note" $w_{\omega_0,t_0}$ is present in the signal $f$, i.e., whether approximately at the time $t_0 + t^*$ the angular frequency $\omega_0 + \omega^*$ is represented in the signal, and if so, with what amplitude and phase.

The approximation error is due to the time duration $D_t(w) > 0$ and the bandwidth $D_\omega(w) > 0$ of the window $w \neq 0$, and thus due to the fact that the values of $w_{\omega_0,t_0}$ and $\widehat{w}_{\omega_0,t_0}$ in the corresponding time-frequency window (see figure) with appropriate weight enter into the integral

$$\widetilde{f}(\omega_0, t_0) = \langle f(s)|w_{\omega_0,t_0}(s)\rangle = (2\pi)^{-1}\langle \widehat{f}(\omega)|\widehat{w}_{\omega_0,t_0}(\omega)\rangle.$$

The smaller $D_t(w)$ is, the better $\widetilde{f}(\omega, t_1)$ and $\widetilde{f}(\omega, t_2)$ can be distinguished for adjacent time points $t_1$ and $t_2$, i.e., the more easily the frequencies present in the signal can be assigned to the different times at which they occur. Therefore, the smaller $D_t(w)$ is, the better the time resolution by $\widetilde{f}$. The smaller the bandwidth $D_\omega(w)$ is, the better the corresponding resolution of different frequencies. However, as we saw in the last section, the quality of a simultaneous time-frequency localization is limited by the uncertainty relation $D_t(w)D_\omega(w) \geqslant 1/2$. The best compromise with regard to the uncertainty relation is therefore the windowed Fourier transform with Gaussian windows proposed by Dennis Gabor (1900-1979), known as the Gabor transform (see p. 377).

**Example.** A short-term model for a siren tone or chirp is approximately the function $f(t) = A\sin(g(t))$ with $g(t) = 2\pi t\left(\alpha t + \beta t^2\right)$ for $0 \leqslant t \leqslant 10$ s and constants $A$, $\alpha$, $\beta$. The derivative of the argument $g'(t) = 2\pi t(2\alpha + 3\beta t)$ can be considered as the instantaneous angular frequency at time $t$. The magnitude spectrum, approximately calculated with $A = 1$, $\alpha = 4$ $[1/s^2]$, $\beta = -4/15$ $[1/s^3]$ over $T = 10$ s, shows a multitude of frequencies up to the maximum frequency 20 Hz, but not the parabolic frequency modulation and not the instantaneous frequencies at different times (left image below). The graph of an approximation for $|\widetilde{f}|$, $\widetilde{f}$ the windowed Fourier transform of $f$ with the "Hann window" $w(t) = 0.5 - 0.5\cos(\omega_0 t)$ for

$0 \leqslant t \leqslant 1$ s, $w(t) = 0$ otherwise ($\omega_0 = 2\pi$ rad/s), on the other hand, clearly shows the rise and fall of the instantaneous frequencies and corresponds to our usual impression of the variable frequency of the siren tone (right image). For the calculation of the approximations of $|\widehat{f}|$ and $|\widetilde{f}|$ with the DFT, also compare p. 325 and the following Section 12.6. For Fig. 12.15 a 512-point DFT was used over a total of $T = 10$ s, with the DFT coefficients $|\widehat{c}_k T|$ plotted as an approximation for $|\widehat{f}(2\pi k/T)|$. In the second case, 50 Hann windows of duration 1 s were used at intervals of 0.2 s each. Per time segment, a 128-point DFT was performed and the resulting (single-sided) DFT magnitude spectra were combined to form the second image in Fig. 12.16. Neither representation shows the constant amplitude $A = 1$. One reason is the strong aliasing effects due to the frequency modulation. The sum of the $|\widehat{c}_k|^2$ of the left image agrees numerically very well with the quadratic mean of $f$ in $[0, T]$ (in both cases, the value is about 0.5). Numerical integration to calculate $|\widetilde{f}|$ for 20 Hz at $t_0 = 5$ s results in approximately 0.24, as shown in the following spectrogram on the right. The signal values (and thus A) can only be approximately recovered from the signal DFT using an interpolation polynomial or the formula for discrete reconstruction from the data on page 387. At end of the book on page 451 you will see another spectrogram of a piece of music like the right image here.

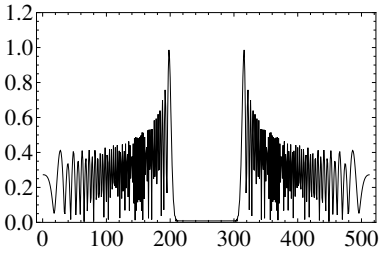


**Fig. 12.15.** DFT of the siren signal

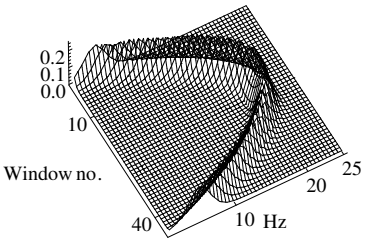


**Fig. 12.16.** STFT of the siren signal

## Reconstruction of a Signal from its Windowed Fourier Transform

For a fixed chosen window $w \neq 0$, let now the transform $\mathcal{G}_w f = \widetilde{f}$ of a signal $f$ be given. An inverse formula for reconstructing the original signal $f$ from the values of $\widetilde{f}$ can be obtained by representing the local part $f_s(t) = \overline{w(t-s)} f(t)$ as a Fourier integral. For fixed $s \in \mathbb{R}$, $\widetilde{f}(\omega, s)$ is the Fourier transform of $f_s(t)$:

$$\widetilde{f}(\omega, s) = \widehat{f}_s(\omega) = \langle f(t) | w(t-s)\, \mathrm{e}^{j\omega t} \rangle = \langle f(t) \overline{w(t-s)} |\, \mathrm{e}^{j\omega t} \rangle.$$

According to our assumptions about $f$ and $w$ (cf. p. 382), $f_s$ is integrable in $t$ and piecewise continuously differentiable, so that with the Fourier inversion formula for

each continuity point $t$ of $f$ (cf. p. 251), it holds

$$\overline{w(t-s)}f(t) = f_s(t) = \frac{1}{2\pi}\int_{-\infty}^{+\infty} \widetilde{f}(\omega, s)\,\mathrm{e}^{j\omega t}\,\mathrm{d}\omega\,.$$

Multiplying both sides of this equation with $w(t-s)$, then integrating with respect to $s$, and dividing by $\|w\|^2$ gives, due to $\int_{-\infty}^{+\infty} |w(t-s)|^2\,\mathrm{d}s = \|w\|^2$, the desired reconstruction formula.

**Theorem 12.5** (Pointwise Reconstruction Formula.)**.** *At each continuity point $t$ of a piecewise continuously differentiable, square-integrable function $f$, the value $f(t)$ can be recovered from the windowed Fourier transform of $f$ by*

$$f(t) = \frac{1}{2\pi\|w\|^2}\int_{-\infty}^{+\infty}\int_{-\infty}^{+\infty} \widetilde{f}(\omega, s)w(t-s)\,\mathrm{e}^{j\omega t}\,\mathrm{d}\omega\,\mathrm{d}s\,.$$

*At discontinuity points $t$ of $f$, the right side gives, as in the Fourier inversion formula, the value $[f(t+) + f(t-)]/2$.*

If $\widetilde{f}(\omega, s) = \langle f(t)|w_{\omega,s}(t)\rangle$ is understood as the projection of the signal onto its time-frequency components, then the reconstruction formula is the "back-projection" by which the signal is recovered from the superposition of its components.

**Remarks.** From $\|w\|^2\langle f(t)|f(t)\rangle = \int_{-\infty}^{+\infty}\int_{-\infty}^{+\infty} |f_s(t)|^2\,\mathrm{d}t\,\mathrm{d}s < \infty$ it follows that the functions $f_s$ are square-integrable with respect to $t$ for almost all $s$ (cf. Appendix B, Fubini's theorem). Applying the Plancherel equation to the inner integral then gives with $w \neq 0$

$$\|f\|^2 = \frac{1}{2\pi\|w\|^2}\int_{-\infty}^{+\infty}\int_{-\infty}^{+\infty} |\widetilde{f}(\omega, s)|^2\,\mathrm{d}\omega\,\mathrm{d}s = \frac{1}{2\pi\|w\|^2}\|\widetilde{f}\|^2.$$

This equation corresponds to the Plancherel equation for the Fourier transform and implies that the windowed Fourier transform $\mathcal{G}_w$ can be extended to a continuous injective mapping defined on the whole $L^2(\mathbb{R})$ into $L^2(\mathbb{R}^2)$ (cf. p. 287). The image $V = \mathcal{G}_w(L^2(\mathbb{R}))$ is a closed subspace of $L^2(\mathbb{R}^2)$, and any function $h \in L^2(\mathbb{R}^2)$ can be uniquely decomposed (cf. p. 55 and later 14.1, p. 419) in the form $h = h_V + h_V^\perp$ with $h_V \in V$ and

$$\langle v|h_V^\perp\rangle = \int_{-\infty}^{+\infty}\int_{-\infty}^{+\infty} v(\omega, s)\overline{h_V^\perp(\omega, s)}\,\mathrm{d}\omega\,\mathrm{d}s = 0.$$

The function $h_V$ is the orthogonal projection of $h$ onto $V$. The adjoint operator $\mathcal{G}_w^*$ to the operator $\mathcal{G}_w$ is defined by the equation $\langle f|\mathcal{G}_w^* g\rangle = \langle \mathcal{G}_w f|g\rangle$. From $\|f\|^2 = (2\pi\|w\|^2)^{-1}\|\widetilde{f}\|^2$ it follows with the polarization equation (p. 263) that $\langle f_1|f_2\rangle = (2\pi\|w\|^2)^{-1}\langle f_1|\mathcal{G}_w^*\mathcal{G}_w f_2\rangle$ for all $f_1, f_2 \in L^2(\mathbb{R})$. Thus, $f = (2\pi\|w\|^2)^{-1}\mathcal{G}_w^*\mathcal{G}_w f$ holds for all $f \in L^2(\mathbb{R})$. The inverse transform to $\mathcal{G}_w$ is therefore the restriction of $(2\pi\|w\|^2)^{-1}\mathcal{G}_w^*$ to the image $V$ of $\mathcal{G}_w$. For the signals we consider, it is given as an integral transformation by the right side of the reconstruction formula. If $h \in L^2(\mathbb{R}^2)$ has the decomposition $h = h_V + h_V^\perp$ with the part $h_V^\perp$ orthogonal to $V$, then $\langle f|\mathcal{G}_w^* h_V^\perp\rangle = \langle \mathcal{G}_w f|h_V^\perp\rangle = 0$ for all $f \in L^2(\mathbb{R})$, thus $\mathcal{G}_w^* h_V^\perp = 0$. With $f = (2\pi\|w\|^2)^{-1}\mathcal{G}_w^* h_V$, $\mathcal{G}_w f = h_V$, it follows

$$(2\pi\|w\|^2)^{-1}\mathcal{G}_w\mathcal{G}_w^* h = (2\pi\|w\|^2)^{-1}\mathcal{G}_w\mathcal{G}_w^* h_V = h_V.$$

The orthogonal projection of $L^2(\mathbb{R}^2)$ onto $V$ is thus the mapping $(2\pi\|w\|^2)^{-1}\mathcal{G}_w\mathcal{G}_w^*$. For more detailed information about adjoint operators and orthogonal projections, see for example J. Weidmann (1980).

With these remarks, it can be seen how desired time-frequency properties can be approximated in signal processing.

## Signal Processing with Windowed Fourier Transforms

Given a windowed Fourier transform $\mathcal{G}_w$ for a fixed chosen window $w \neq 0$. Since the functions $\mathcal{G}_w f$, $f \in L^2(\mathbb{R})$, are bounded and $L^2(\mathbb{R}^2)$ also contains unbounded functions, not every square-integrable function $h(\omega, t)$ can be the windowed Fourier transform of a function $f \in L^2(\mathbb{R})$:
$V = \mathcal{G}_w(L^2(\mathbb{R})) \neq L^2(\mathbb{R}^2)$. Otherwise, signals with arbitrary time-frequency properties could be constructed – in contradiction to Heisenberg's uncertainty principle. However, one can proceed as follows to obtain signals that approximate the desired time-frequency properties as closely as possible:

For a given signal $f(t)$, the windowed Fourier transform $\widetilde{f} = \mathcal{G}_w f$ is computed and $\widetilde{f}$ is processed as desired to $h$ from $L^2(\mathbb{R}^2)$, for example by filtering, shifting values, amplifying, etc. The function $h$ is the model of the desired time-frequency properties. However, in general, there is no signal $g$ such that $h = \mathcal{G}_w g$. The signal $f_h$ in $L^2(\mathbb{R})$, whose time-frequency properties are very close to those of $h$, is $f_h = (2\pi\|w\|^2)^{-1}\mathcal{G}_w^* h$, because according to the preceding remarks, the function $\widetilde{f_h}$ as the orthogonal projection of $h$ onto $V$ minimizes the mean square error $\|h - \widetilde{f}\|$, $f \in L^2(\mathbb{R})$ (cf. also later 14.1, p. 419).

## Discrete Windowed Fourier Transform

Of great importance for numerical approximation and thus for digital signal processing is the question of whether a signal can be reconstructed from the sampled values of its windowed Fourier transform. We present a sampling theorem and illustrate some fundamental aspects of discrete time-frequency analysis with windowed Fourier transforms.

Under the same conditions as for the reconstruction formula on p. 385, we assume that the window function $w \neq 0$ vanishes outside an interval $[a, b]$. For a fixed value of $s$, the support of $f_s(t) = \overline{w(t-s)} f(t)$ is contained in $[a+s, b+s]$. Fourier series expansion of $f_s$ in this interval yields for each continuity point $t$ of $f$ in $[a+s, b+s]$

$$f_s(t) = \sum_{k=-\infty}^{+\infty} c_k(s)\, \mathrm{e}^{jk\omega_0 t} \quad \text{with} \quad \omega_0 = \frac{2\pi}{b-a}\,,$$

$$c_k(s) = \frac{1}{b-a} \int_{a+s}^{b+s} f(t)\overline{w(t-s)}\, \mathrm{e}^{-jk\omega_0 t}\, \mathrm{d}t = \frac{\omega_0}{2\pi} \widetilde{f}(k\omega_0, s).$$

Multiplying $f_s(t)$ by $w(t-s)$ results in the functions $w_{k\omega_0,s}$, which were defined by $w_{k\omega_0,s}(t) = w(t-s)\, \mathrm{e}^{jk\omega_0 t}$:

$$|w(t-s)|^2 f(t) = \frac{\omega_0}{2\pi} \sum_{k=-\infty}^{+\infty} \widetilde{f}(k\omega_0, s) w_{k\omega_0,s}(t).$$

Instead of integrating this equation over $s$ and dividing by $\|w\|^2$ as in the reconstruction formula on p. 385, we form a discrete approximation for $\|w\|^2 = \int_{-\infty}^{+\infty} |w(t-s)|^2\, \mathrm{d}s$ by $A_{t_0}(t) = t_0 \sum_{n=-\infty}^{+\infty} |w(t-nt_0)|^2$ and sum over $s_n = nt_0$, $n \in \mathbb{Z}$:

$$A_{t_0}(t) f(t) = \frac{\omega_0 t_0}{2\pi} \sum_{n=-\infty}^{+\infty} \sum_{k=-\infty}^{+\infty} \widetilde{f}(k\omega_0, nt_0) w_{k\omega_0, nt_0}(t).$$

Due to the limited support of $w$, the series for $A_{t_0}(t)$ has only finitely many non-zero terms. Now we obtain the desired sampling theorem, i.e., a discrete reconstruction formula under the condition $A_{t_0}(t) \neq 0$:

**Theorem 12.6** (Discrete Reconstruction)**.** *If $A_{t_0}(t) \neq 0$ everywhere, then the signal $f$ is given at each continuity point $t$ by*

$$f(t) = \frac{\omega_0 t_0}{2\pi} \sum_{n=-\infty}^{+\infty} \sum_{k=-\infty}^{+\infty} \widetilde{f}(k\omega_0, nt_0) w_{k\omega_0, nt_0}(t) A_{t_0}(t)^{-1}.$$

The better the time-frequency localization of $w$, the faster the values $|w_{k\omega_0,nt_0}(t)|$ will decrease. In practice, for bandlimited signals $f$, finite partial sums of the right side with discrete approximations of the values of $\widetilde{f}$ yield good approximations for $f(t)$.

From the derivation of the formula, the following conditions for a stable reconstruction are determined:

1. For numerically stable reconstruction, it is not enough to require $A_{t_0}(t) > 0$, but $\inf_{t\in\mathbb{R}} A_{t_0}(t) > 0$. Otherwise, small errors in the calculation of the values $\widetilde{f}(k\omega_0, nt_0)$ would lead to very large errors in $f(t)$ at points $t$ where the value of $A_{t_0}(t)$ is very close to zero. This is a condition on the sampling rate because $\lim_{t_0\to 0+} A_{t_0}(t) = \|w\|^2 \neq 0$ holds for all $t$ if the window is assumed to be continuous. Thus, this stability condition can be maintained for sufficiently small $t_0$.
2. A necessary condition for $A_{t_0}(t) > 0$ is $0 < t_0 \leqslant b - a$, otherwise $A_{t_0}(t) = 0$ for $b < t < a + t_0$. The given discrete reconstruction is therefore certainly *not* possible if $\omega_0 t_0 > 2\pi$.

Such conditions are typical when searching for stable discrete reconstruction formulas. Considering window functions $w$ that are not time-limited, we will analogously demand, as in point 1, that $\sup_{t\in\mathbb{R}} A_{t_0}(t) < \infty$ and that both this upper bound and the lower bound from point 1 converge to $\|w\|^2$ as $t_0 \to 0+$.

The mathematical task in the search for sampling formulas is to find conditions on the window function and the set of sampling points $(k\omega_0, nt_0)$, $k, n \in \mathbb{Z}$, such that the operator $\mathcal{G}_w^{\omega_0,t_0}$, which maps a signal to the sequence $(\langle f(t)|w_{k\omega_0,nt_0}(t)\rangle)_{k,n\in\mathbb{Z}}$, is injective. To obtain numerically stable formulas, $\mathcal{G}_w^{\omega_0,t_0}$ must additionally be continuous in an appropriate sense and have a continuous inverse mapping. This task leads in modern signal processing to the study of complete orthonormal systems in suitable function spaces. Instead of pointwise convergent sampling series, we then consider series that approximate the analyzed signals in the norm of the function space used. The considered signals can also be functions $f(t, \mathbf{x})$ that depend not only on time $t$ but also on a spatial variable $\mathbf{x}$. Such signals appear, for example, in image processing. Accordingly, systems of functions with multiple variables are used. Readers who find this section a motivation to delve deeper into the subject, given the importance of digital signal processing in audio and video technology but also in many other areas of engineering and natural sciences, are referred to further literature, such as I. Daubechies (1992), H. G. Feichtinger, T. Strohmer (2003), K. ayöchenig (2001), or Y. Meyer (1993).

*Finally, some central results of discrete time-frequency analysis with windowed Fourier transforms are cited:*

1. If the product $\omega_0 t_0 > 2\pi$ holds, then for any choice of window $w$, there are always signals $f \in L^2(\mathbb{R})$, $f \neq 0$, that are orthogonal to all functions $w_{k\omega_0,nt_0}$. Therefore, a reconstruction of such signals from their windowed Fourier trans-

forms $\mathcal{G}_w^{\omega_0,t_0} f$ is not possible. Discrete reconstruction formulas are generally subject to the condition $\omega_0 t_0 \leqslant 2\pi$.

2. If the function system $w_{k\omega_0,nt_0}$, $k,n \in \mathbb{Z}$, forms a complete orthogonal system in $L^2(\mathbb{R})$, then necessarily $\omega_0 t_0 = 2\pi$ must hold.
3. Even for $\omega_0 t_0 = 2\pi$, the functions $w_{k\omega_0,nt_0}$, $k,n \in \mathbb{Z}$, with the Gaussian window proposed by D. Gabor $w(t) = (2\pi)^{-1/4}\,\mathrm{e}^{-t^2/4}$ do not form an orthonormal system in $L^2(\mathbb{R})$. It can be shown that

$$\inf\left\{\|f\|^{-2}\sum_{k,n\in\mathbb{Z}} |\langle f|w_{k\omega_0,nt_0}\rangle|^2 \;:\; f\in L^2(\mathbb{R}), f\neq 0\right\} = 0$$

holds. Although the functions $w_{k\omega_0,nt_0}$, $k,n \in \mathbb{Z}$, form a *complete system* in $L^2(\mathbb{R})$ (i.e., any $f \in L^2(\mathbb{R})$ can be approximated arbitrarily well by linear combinations of the $w_{k\omega_0,nt_0}$ with respect to the norm of $L^2(\mathbb{R})$), a numerically stable reconstruction of signals $f \in L^2(\mathbb{R})$ from the coefficients $\langle f|w_{k\omega_0,nt_0}\rangle$ is generally not possible.
4. While orthogonality relations for the functions $w_{k\omega_0,nt_0}$ would be desirable, practical requirements for good time-frequency localization of the windows even force $\omega_0 t_0 < 2\pi$, i.e., higher sampling rates are necessary than those that allow for the orthogonality of the system $w_{k\omega_0,nt_0}$. This statement is contained in the **uncertainty principle of R. Balian and F. Low**:
*If the functions $w_{k\omega_0,nt_0}$ form a complete orthonormal system in $L^2(\mathbb{R})$ for a window $w \in L^2(\mathbb{R})$ with $\omega_0 t_0 = 2\pi$, then it holds that*

$$\int_{-\infty}^{+\infty} t^2|w(t)|^2\,\mathrm{d}t = \infty \quad \text{or} \quad \int_{-\infty}^{+\infty} \omega^2|\widehat{w}(\omega)|^2\,\mathrm{d}\omega = \infty.$$

5. For $\omega_0 t_0 < 2\pi$, there are windows $w$ and corresponding complete function systems (so-called *Gabor frames*) $w_{k\omega_0,nt_0}$, $k,\ n \in \mathbb{Z}$, that enable stable reconstruction with very good time-frequency localization, i.e., with

$$\int_{-\infty}^{+\infty} t^2|w(t)|^2\,\mathrm{d}t < \infty \quad \text{and} \quad \int_{-\infty}^{+\infty} \omega^2|\widehat{w}(\omega)|^2\,\mathrm{d}\omega < \infty.$$

A derivation and detailed discussion of these results can be found, for example, in the already mentioned book of I. Daubechies (1992) or in K. Gröchenig (2001). Aspects of the window functions when using the DFT to approximate windowed Fourier transforms are discussed in the following section.

## 12.6 Time Windows with the Discrete Fourier Transform

In practice, the spectrum of a signal $f$ can often not be calculated exactly. Instead, one usually uses the spectral function of a signal segment $fw_T$ with a time window $w_T \neq 0$ as an approximation. Also, when analyzing unknown signals $f$, the observation duration $T$ is necessarily finite, so that only information about time segments $fw_T$ can be processed. In time-frequency analysis, as in the last section, the interest is also in the spectral functions of such time segments of the signal.

For the approximate calculation of the Fourier transform of $fw_T$, the discrete Fourier transform is often used (see p. 325 and Section 6). The spectrum $\widehat{fw_T}$ of the signal segment $fw_T$ is different from the actual spectrum $\widehat{f}$ of $f$. If $w_T$ is a time window with support in $[0, T]$, then according to the modulation theorem from p. 262 for square-integrable or bandlimited signals $f$

$$\widehat{fw_T} = \frac{1}{2\pi} \widehat{f} * \widehat{w_T}. \tag{12.1}$$

The spectral function of $fw_T$ is compared to $\widehat{f}$ "smeared, smoothed, and blurred" due to the convolution of $\widehat{f}$ with $\widehat{w_T}$. The shorter the observation duration $T$, the greater the bandwidth of $w_T$ according to the uncertainty principle, and the worse the frequency localization of $w_T$ and thus of $fw_T$ (see 12.4 and 12.5). A typical problem is then, for example, the resolution of periodic signal components of closely adjacent frequencies, especially when these signal components have very different amplitudes.

The observation duration $T$ and the shape of the time window $w_T$ also have an impact on the quality of the approximations for $\widehat{fw_T}$, which are obtained with a finite discrete Fourier transform from sampled values of $fw_T$. Therefore, when using the discrete Fourier transform, some fundamental aspects of the interaction between the observation duration $T$, the properties of the weighting function $w_T$, and the sampling rate used for the discrete Fourier transform must be considered.

### Truncation Effects in the Discrete Fourier Transform

In the discrete Fourier transform, from finitely many values $y_n = f(n\Delta t)$, $\Delta t > 0$, $n = 0, \ldots, N-1$, of a signal $f$ the Fourier coefficients

$$\widehat{c}_k = \frac{1}{N} \sum_{n=0}^{N-1} y_n \, \mathrm{e}^{-jkn2\pi/N}$$

are calculated for $k = 0, \ldots, N-1$ (see 6, p. 78). We assume the signal $f$ to be continuous in $[0, T[$ with the limit value $f(T-)$ and piecewise continuously differentiable. The sampled time section of $f$ beyond the sampling period of duration $T_a = (N-1)\Delta t$ can be arbitrarily extended to a periodic function $f_p$ with the pe-

riod $p = N\Delta t = T$, for example as in the following figure, where we have added a straight segment between $T_a$ and $T$ so that $f_p$ becomes continuous (see Fig. 12.17).

Let us denote by $w_T$ the *rectangle window*

$$w_T(t) = 1 \text{ for } 0 \leqslant t < T,\ w_T(t) = 0 \text{ otherwise,}$$

then the quantities $\widehat{c}_k$ are on one hand approximations for Fourier coefficients $c_k(f_p)$ of $f_p$, and on the other hand, according to p. 324, they also yield approximations for sample values of $\widehat{fw_T}$ and thus approximations for the Fourier coefficients $c_k = c_k(fw_T)$ of $fw_T$. In many applications $\widehat{c}_k T$ also serves as an estimator for $\widehat{f}(2\pi k/T)$ (see also Exercise A4 of Chapter 11).


**Fig. 12.17.** Last sample time is $T_a < T$, a possible $T$-periodic extension could be $f_p$

If, for instance, $N$ is an even number, then one uses the value $\widehat{c}_k$ for the indices $k = 0, \ldots, (N-2)/2$ respectively as an approximation for the Fourier coefficient $c_k$ of $fw_T$. For $k = (N+2)/2, \ldots, N-1$, $\widehat{c}_k$ serves accordingly as an approximation for $c_{-N+k}$ and $\widehat{c}_{N/2}$ as an approximation for $(c_{-N/2} + c_{N/2})/2$ (see p. 80). The corresponding oscillations to the fundamental circular frequency $\omega_0 = 2\pi/T$

$$\begin{aligned} v_0(t) = 1,\ v_1(t) = \mathrm{e}^{j\omega_0 t}, \ldots, v_{(N-2)/2}(t) = \mathrm{e}^{j(N-2)\omega_0 t/2},\ v_{N/2}(t) \\ = \cos(N\omega_0 t/2), v_{(N+2)/2}(t) = \mathrm{e}^{-j(N-2)\omega_0 t/2}, \ldots\ldots, v_{N-1}(t) = \mathrm{e}^{-j\omega_0 t}, \end{aligned}$$

generate an $N$-dimensional function vector space $V$ in $L^2([0,T])$ (see p. 12).
For the rectangle window $w_T$, the $T$-periodic extension of $fw_T$ has jump discontinuities at $t = kT$, $k \in \mathbb{Z}$, if $f(0) \neq f(T-)$. According to p. 78, with continuous $f_p$ as above, the aliasing relationships hold

$$\widehat{c}_k = \sum_{m=-\infty}^{+\infty} c_{k+mN}(fw_T) + \frac{1}{2N}\left(f(0) - f(T\text{-})\right) = \sum_{m=-\infty}^{+\infty} c_{k+mN}(f_p). \quad (12.2)$$

If the signal $f$ is a mixture of harmonic oscillations with circular frequencies $k\omega_0$, $k = 0, \ldots, N/2$, i.e., if $f(t) = \sum_{k=0}^{N-1} \alpha_k v_k(t)$ is a linear combination of the functions $v_0, \ldots, v_{N-1}$, then $f(0) = f(T-)$ and with the inner product from p. 12 it follows from the aliasing relationship (12.2)

$$\widehat{c}_k = \langle f(t)|v_k(t)\rangle = \frac{1}{T}\int_0^T f(t)\overline{v_k(t)}\,\mathrm{d}t = \alpha_k. \tag{12.3}$$

The orthogonal projections of $f$ onto the one-dimensional subspaces of $V$ generated by the functions $v_k$ then yield the exact spectral values of $f$.

It is different if the periodic extension of $fw_T$ has a jump discontinuity at $t = T$ or if the originally observed signal $f$ contains harmonic oscillations whose period duration does not match $T$. In practice, this will often be the case when analyzing unknown signals $f$, which are sampled over an arbitrarily chosen time period. Simple examples of such cases are given by the functions $f_1(t) = \cos(t)$ and $f_2(t) = -\cos(t/2) + \cos(t)/2$. For $T = \pi$, the $T$-periodic extension of $f_1 w_T$ with the rectangle window $w_T$ has a jump discontinuity at $T$, while that of $f_2 w_T$ is continuous, but $f_2$ is not $T$-periodic.

If $fw_T(0) \neq fw_T(T-)$, then every $T$-periodic extension, $T = N\Delta t$, of $f$ beyond the interval $[0, T_a]$, $T_a = (N-1)\Delta t$, has jump discontinuities or steep flanks in the vicinities of the points $kT$, $k \in \mathbb{Z}$ (see last figure). From considerations on the asymptotics of Fourier coefficients (p. 44), it follows that the magnitudes of the coefficients $c_k$ of a $T$-periodic extension of the signal section for $|k| \to \infty$ decrease only slowly. Consequences are, according to equation (12.2), aliasing effects in the coefficients $\widehat{c}_k$ of the discrete Fourier transform.

Even if by chance $fw_T(0) = fw_T(T-)$ as in the example $f_2 w_T$ above, aliasing effects arise as soon as $f$ contains oscillation components with frequencies $\nu \neq k/T$, and also if they lie within the Nyquist interval with the cutoff frequency $N/(2T)$.

*Every signal component with a circular frequency $\omega_1 \neq 2\pi k/T$ has non-zero projections in all subspaces of $L^2([0,T])$, which are generated by the functions $v_k$ for $k = 0, \ldots, N-1$:*

$$\langle \mathrm{e}^{j\omega_1 t}\, w_T(t)|v_k(t)\rangle \neq 0 \text{ for all } k = 0, \ldots, N-1.$$

**Example.** Consider for example the signal $g(t) = A\,\mathrm{e}^{j\omega_1 t}$, then for the $k$-th Fourier coefficient $c_k(gw_T)$ of $gw_T$ with the rectangle window $w_T$ for the interval $[0, T[$ according to (12.1) and p. 324 with $\widehat{g}(\omega) = 2\pi A\delta(\omega - \omega_1)$:

$$\begin{aligned} c_k(gw_T) &= \frac{1}{T}\widehat{gw_T}\left(\frac{2\pi k}{T}\right) = \frac{1}{2\pi T}(\widehat{g} * \widehat{w_T})\left(\frac{2\pi k}{T}\right) \\ &= \frac{A}{T}\,\mathrm{e}^{-j(2\pi k/T-\omega_1)T/2}\,\widehat{w_T}\left(\frac{2\pi k}{T} - \omega_1\right) \\ &= (-1)^k A\,\mathrm{e}^{j\omega_1 T/2}\,\frac{\sin(\pi k - \omega_1 T/2)}{\pi k - \omega_1 T/2}. \end{aligned} \tag{12.4}$$

These coefficients distort, as per (12.2), the amplitudes and phases of the estimates $\widehat{c}_k$ of signal components at frequencies $k/T$, $k \leqslant N/2$, when $\omega_1 \neq 2\pi k/T$. When

using the rectangular window according to (12.2) and (12.4), they contribute as alias effects to all DFT coefficients $\widehat{c}_k$. Thus, they are "spread" onto the oscillations at frequencies $k/T$ (see the next figure). This phenomenon is referred to in signal processing as the *spectral leakage effect*. Additionally, for all $\widehat{c}_k$, there is a constant additive component $(g(0) - g(T-))/(2N)$ if the $T$-periodic extension of $gw_T$ at $T$ has a jump discontinuity.

The spectral leakage effect occurs with modified coefficients $c_k(gw_T)$ even when using other window functions $w_T$ instead of the rectangular window, and it results from the uncertainty principle for the time-duration-bandwidth product of the window $w_T$.

The following Fig. 12.18 shows some absolute weights $g_k = |c_k(gw_T)/A|$, through which the amplitude $A$ of $gw_T$ is distributed onto the Fourier coefficients of angular frequencies $2\pi k/T$ adjacent to $\omega_1$ by the periodicity induced by $w_T$.

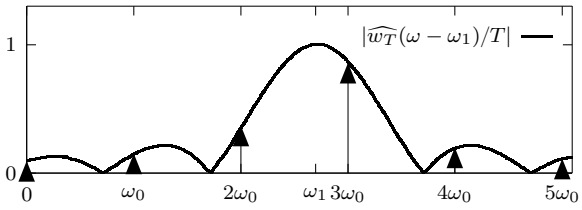


**Fig. 12.18.** The arrows show the absolute weights $g_k$ at $k\omega_0$

We briefly consider an example that illustrates the discussed truncation effects due to the rectangular window using specific data for a given signal $f$.

**Example.** For the $4\pi$-periodic function $f(t) = \cos(t/2)$, the segment $fw_T$ with the rectangular window $w_T$ of length $T = \pi$ has the spectrum $c_k = -\dfrac{2 + 8kj}{\pi(16k^2 - 1)}$. The $\pi$-periodic extension with $fw_T(0) = fw_T(\pi)$ has the mean value $c_0 = 2/\pi$ on $[0, \pi[$ and jump discontinuities of height $S_1 = 1$ at $t = k\pi$ ($k \in \mathbb{Z}$). A 3-point DFT on $[0, \pi[$ yields the DFT coefficients $\widehat{c}_0 = (3 + \sqrt{3})/6$ and $\widehat{c}_1 = \overline{\widehat{c}_2} = (3 - \sqrt{3})/12 - j(3 - \sqrt{3})/12$.

We specifically examine $\widehat{c}_0$. The series $\displaystyle\sum_{m=1}^{\infty}(c_{3m} + c_{-3m}) = -\frac{4}{\pi}\sum_{m=1}^{\infty}\frac{1}{144m^2 - 1}$ has, according to (11.2), the limit $S_2 = \widehat{c}_0 - c_0 - S_1/6 = -\dfrac{2}{\pi} + \dfrac{2 + \sqrt{3}}{6}$. Using known equations for the digamma function $\Psi = \Gamma'/\Gamma$, $S_2$ can also be obtained as

$$S_2 = \frac{\Psi(11/12) - \Psi(1/12) - 12}{6\pi} = -\frac{2}{\pi} + \frac{\cot(\pi/12)}{6}.$$

In decimal approximation, for $\widehat{c}_0$ the decomposition now yields

$$\widehat{c}_0 = c_0 + S_1/6 + S_2 \approx 0.636619 + 0.166667 - 0.014611 = 0.788675.$$

## Selection of Time Windows in the Discrete Fourier Transform

By choosing an appropriate window function $w_T$, one can achieve a reduction of the distortion effects in the spectrum of the discrete Fourier transform and thereby reduce the error in estimating the spectrum of $fw_T$ or of $f$. The frequency localization is better, according to the considerations on the uncertainty principle in Section 12.4, the faster $|\widehat{w_T}(\omega)|$ decreases for increasing $|\omega|$.

1. One usually chooses a window function $w_T \neq 0$ that is as smooth as possible with support in $[0, T]$ and $w_T(0) = w_T(T) = 0$. Then the $T$-periodic extension of $fw_T$ for continuous signals $f$ has no jump discontinuities, and the aliasing effects described by formula (12.2) are reduced if the Fourier coefficients of this extension decrease rapidly (cf. 4.5). One then obtains a better estimate with $\widehat{c}_k T$ than with the rectangular window for the value $\widehat{f}(2\pi k/T)$, which is often sought in applications.
2. One chooses the observation duration $T$ to be as long as possible. The smaller $T$ is, the larger the bandwidth of $w_T$, i.e., the worse the frequency localization.
3. One chooses the number $N$ of samples to be as high as possible. More signal frequencies are then resolved exactly (cf. Equation (12.3)). For fully observed time-limited signals, "zero padding" improves the approximations for $\widehat{f}$.
4. The leakage effect is less significant, the faster the side lobes of $|\widehat{w_T}|$ decrease compared to the main lobe (cf. the preceding image). Therefore, window functions are often chosen where these side lobes of $|\widehat{w_T}|$ decrease rapidly.

In practice, many different weighting functions $w_T$ are used. The use of special window functions and thus the compromise that must always be made due to the uncertainty principle depends on the aim of the respective application. Criteria besides the decay behavior of $\widehat{w_T}$ and the bandwidth of the window include, for example, its energy concentration in a given frequency band or simple calculation and implementation possibilities in software applications. A detailed comparative discussion of commonly used window functions can be found, for example, in D. Slepian (1983) or in F. Harris (1978).

**Example.** To conclude, we consider as an illustrative example the signal

$$f(t) = A_1 \cos(2\pi\nu_1 t) + A_2 \cos(2\pi\nu_2 t)$$

with $A_1 = 1$, $A_2 = 0.03$, $\nu_1 = 10.25\,\text{Hz}$, and $\nu_2 = 12\,\text{Hz}$. Fig. 12.19 shows the discrete Fourier transform with the rectangular window $w_T$, $T = 2\,\text{s}$, for $N = 128$. The signal frequency $\nu_2$ cannot be detected. With the same $T$ and $N$, the often-used *Hann window* $w_T$,

$$w_T(t) = 0.5 - 0.5\cos(2\pi t/T), \;\; 0 \leqslant t \leqslant T$$

is used in the second Fig. 12.20. In the third Fig. 12.21, this window is used again with $T = 5\,\text{s}$ and $N = 1024$. From the result of this DFT in the third image, the

12 Hz signal frequency can at least be suspected. Displayed is the single-sided DFT magnitude spectrum.

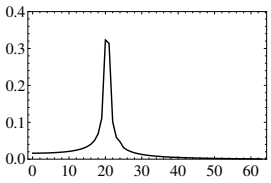


**Fig. 12.19.** 128-point DFT, $T = 2$s, rectangular window

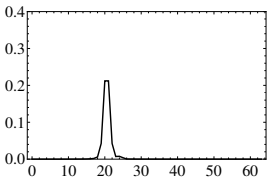


**Fig. 12.20.** 128-point DFT, $T = 2$s, Hann window

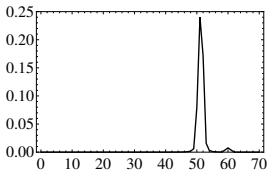


**Fig. 12.21.** 1024-point DFT, $T = 5$s, Hann window

One notices from the graphs that the height of the "peaks" does not correspond to the actual (half) amplitude values of the two oscillations. This is a consequence of the aliasing effect and the attenuations due to the added weighting functions. Therefore, caution is required and additional information about the nature of a problem is needed to reasonably interpret DFT spectra of unknown signals, which are far more complex in practice than this small example and often affected by disturbances.

Next is another, still simple example of a DFT spectrum of a real signal, calculated with the rectangular window. Fig. 12.22 shows the 8820-point DFT of an audio signal of 4 s duration, consisting only of the tones F4, A4, C5, F5 of the F major chord, played on the piano and enriched with the tones F4, Eb5, F5, played on the alto saxophone.

The tones have the frequencies in equal temperament: F4=349.23, A4=440, C5=523.25, Eb5=622.25, and F5=698.46 Hz. With prior knowledge about the signal, one recognizes the played notes (the 2nd octave requires intonation adjustment on the alto sax; the author unfortunately intonated about 8 Hz too high for F5). Likewise, one sees a whole series of resonating overtones (octaves and fifths upward), but also subharmonic frequencies (F3, C4, Eb4) and a broad spectrum of admixtures due to the instrument characteristics and DFT aliasing effects. Imagine the spectrum of a whole orchestra or a band with drums, guitar, bass, and brass section, and consider what a well-trained ear can distinguish while enjoying music.

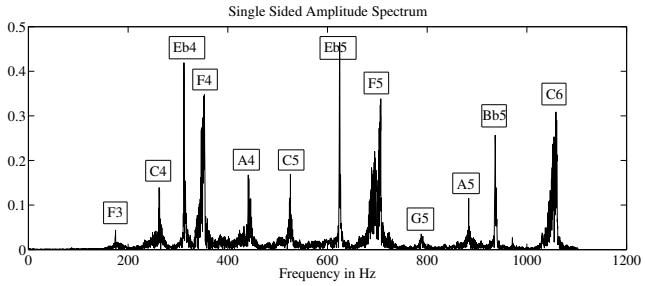


**Fig. 12.22.** 8820-point DFT in 4s with piano and saxophone

## 12.7 Initial Value Problems for Stable LTI Systems

In Section 9.2 we discussed causal initial value problems for differential equations of the form $P(D)u = Q(D)f$ with polynomials $P$ and $Q$ for $t \geqslant 0$ and distributional right-hand sides $f \in \mathcal{D}'_+$. Such problems occur in time-invariant linear transmission systems that have energy storage elements charged at the initial time $t = 0$. The correspondences of the Fourier transform of rational functions on p. 277 show that such problems can also be solved using the Fourier transform if $f$ belongs to the space $\mathcal{S}'_+$, i.e., $f \in \mathcal{S}'$ and $\operatorname{supp}(f) \subset [0, \infty[$, and if further the polynomials $Q$ and $P$ do not have common linear factors and all poles of $Q/P$ have negative real parts.

**Example.**

We will once again treat the $RLC$ oscillating circuit from Example 3 on p. 213 as an example. The differential equation

$$\ddot{U}_a + \frac{2}{\sqrt{LC}}\dot{U}_a + \frac{1}{LC}U_a = U_1\dot{\delta} \text{ and } U_a(0-) = U_0 \ , \ \dot{U}_a(0-) = 0$$

described the oscillating circuit at critical damping ($R^2 = 4L/C$) with input voltage $U_e(t) = U_1 s(t)$ and given initial values. The solution is the voltage progression across the inductance. The homogeneous differential equation is asymptotically stable and the right-hand side is tempered. As in Section 9.2, we are interested in the solution from the initial time $t = 0$ onwards, excluding the past $t < 0$.

The unique solution $T \in \mathcal{S}'$ with $\operatorname{supp}(T) \subset [0, \infty[$ is obtained according to the theorem on p. 206 from the distributional equation

$$\ddot{T} + \frac{2}{\sqrt{LC}}\dot{T} + \frac{1}{LC}T = U_1\dot{\delta} + \frac{2U_0}{\sqrt{LC}}\delta + U_0\dot{\delta}.$$

Since under the given conditions $1/P$ has only poles with negative real parts and hence $1/P(j\omega)$ is a multiplier in $\mathcal{S}'$, Fourier transform of this equation and solving for $\widehat{T}$ gives

$$\widehat{T}(\omega) = \frac{1}{P(j\omega)}\left((U_1 + U_0)j\omega + \frac{2U_0}{\sqrt{LC}}\right).$$

The inverse Fourier transform of the partial fractions using the correspondences from p. 277, left as an exercise for the reader, then yields the same solution $T$ with support in $[0, \infty[$ as on p. 213. Here, as there, $s(t)$ denotes the Heaviside step function.

$$T(t) = \left(U_0 + U_1 + \frac{(U_0 - U_1)t}{\sqrt{LC}}\right)\mathrm{e}^{-t/\sqrt{LC}}\, s(t).$$

For the solution method shown, the condition that all poles of $Q/P$ have negative real parts is not sufficient if $Q$ and $P$ have common linear factors with zeros whose real part $r \geqslant 0$. We consider the following example.

**Example.** The causal time-invariant system on $\mathcal{S}'_+$, described by the differential equation

$$P(D)u = \ddot{u} + \dot{u} - 2u = \ddot{f} + 2\dot{f} - 3f = Q(D)f$$

is stable with vanishing initial values. It has the impulse response

$$h(t) = \delta(t) + \mathrm{e}^{-2t}\, s(t)$$

and the frequency response $\widehat{h}(\omega) = \dfrac{j\omega + 3}{j\omega + 2}$.The general solution of the homogeneous equation $P(D)u = 0$ is $u_H(t) = k_1\,\mathrm{e}^{t} + k_2\,\mathrm{e}^{-2t}$ with $k_1, k_2 \in \mathbb{R}$. The solution $u_H$ is not tempered and for non-vanishing initial values $c_0$, $c_1$ the corresponding causal initial value problem (cf. p. 206)

$$\ddot{u} + \dot{u} - 2u = \ddot{f} + 2\dot{f} - 3f + (c_0 + c_1)\delta + c_0\dot{\delta}$$

in $\mathcal{S}'_+$ cannot generally be solved by Fourier transform. The reason is that with vanishing initial values the common linear factors compensate at the zero $z = 1$ of $P$ and $Q$, while with non-vanishing initial values and proceeding as above, a non-causal solution is obtained.

How initial value problems for certain partial differential equations can also be solved using the Fourier transform is shown in the following section.

## 12.8 Initial Value Problems for 3D Wave and Heat Equations

In previous sections, we solved some boundary value problems for the wave and heat equations using Fourier series. As an application of the Fourier transform, we now obtain solutions of initial value problems for wave and heat equations in unbounded space. Because the Fourier transform converts differentiation into a simple algebraic multiplication operation, it transforms the respective partial differential equations into easily solvable ordinary differential equations.

### The Initial Value Problem for the 3D Homogeneous Wave Equation

The homogeneous wave equation describes, for example, the propagation of small disturbances in frictionless, compressible fluids or gases in the absence of external forces. In homogeneous unbounded isotropic space, the corresponding initial value problem in Cartesian coordinates is given for $u : \mathbb{R}^3 \times [0, \infty[ \to \mathbb{R}$ by

$$\frac{\partial^2 u}{\partial t^2}(\mathbf{x}, t) = c^2 \Delta_{\mathbf{x}} u(\mathbf{x}, t),$$

$$u(\mathbf{x},0) = f(\mathbf{x}), \quad \frac{\partial u}{\partial t}(\mathbf{x},0+) = g(\mathbf{x}), \quad u(\mathbf{x},t) = 0 \text{ for } t < 0. \quad (12.5)$$

Here, $\mathbf{x} \in \mathbb{R}^3$ and $\Delta_{\mathbf{x}}$ is the Laplace operator related to the spatial parameters. If the equation describes, for instance, sound propagation, then $u(\mathbf{x},t)$ is the pressure deviation at time $t$ from the normal atmospheric pressure at location $\mathbf{x}$. The solution $u$ depends on the initial conditions, which we assume to be in $\mathcal{S}(\mathbb{R}^3)$.

The Fourier transform of the equations with respect to the spatial coordinates gives, by interchanging the Fourier integral with differentiation in $t$

$$\begin{aligned}\frac{\partial^2 \widehat{u}}{\partial t^2}(\boldsymbol{\omega},t) &= \frac{\partial^2}{\partial t^2} \int\limits_{\mathbb{R}^3} u(\mathbf{x},t)\, \mathrm{e}^{-j\boldsymbol{\omega}\cdot\mathbf{x}}\, \mathrm{d}\lambda^3(\mathbf{x}) = c^2 \int\limits_{\mathbb{R}^3} \Delta_{\mathbf{x}} u(\mathbf{x},t)\, \mathrm{e}^{-j\boldsymbol{\omega}\cdot\mathbf{x}}\, \mathrm{d}\lambda^3(\mathbf{x}) \\ &= -c^2|\boldsymbol{\omega}|^2 \widehat{u}(\boldsymbol{\omega},t), \quad \widehat{u}(\boldsymbol{\omega},0) = \widehat{f}(\boldsymbol{\omega}), \quad \frac{\partial \widehat{u}}{\partial t}(\boldsymbol{\omega},0+) = \widehat{g}(\boldsymbol{\omega}). \quad (12.6)\end{aligned}$$

For each fixed $\boldsymbol{\omega}$, this is an initial value problem for an ordinary differential equation in $t$. We impose the condition $\widehat{u}(\boldsymbol{\omega},t) = 0$ for $t < 0$. Then we have with the unit step $s(t)$ the unique solution (cf. Theorem 9.5)

$$\widehat{u}(\boldsymbol{\omega},t) = \left( \widehat{f}(\boldsymbol{\omega}) \cos(ct|\boldsymbol{\omega}|) + \widehat{g}(\boldsymbol{\omega}) \frac{\sin(ct|\boldsymbol{\omega}|)}{c|\boldsymbol{\omega}|} \right) s(t).$$

Since $\cos(ct|\boldsymbol{\omega}|) = \dfrac{\mathrm{d}}{\mathrm{d}t} \dfrac{\sin(ct|\boldsymbol{\omega}|)}{c|\boldsymbol{\omega}|}$, it is sufficient to determine the inverse Fourier transform of $\dfrac{\sin(ct|\boldsymbol{\omega}|)}{c|\boldsymbol{\omega}|}$. We already did this on p. 293 and obtain for $t > 0$:

$$\frac{1}{4\pi c^2 t} \delta(|\mathbf{x}| - ct) \circ\!\!-\!\!\bullet \frac{\sin(ct|\boldsymbol{\omega}|)}{c|\boldsymbol{\omega}|}. \quad (12.7)$$

$\delta(|\mathbf{x}| - ct)$ is the singular distribution given by the integral over the spherical surface $|\mathbf{x}| = ct$. By the convolution theorem, we obtain $u$ referred to as a wave. Since the Fourier transform is one-to-one, this $u$ is a unique solution of (12.5).

**Theorem 12.7.** *The initial value problem (12.5) for the wave equation in space has for $\mathbf{x} \in \mathbb{R}^3$ and $t > 0$ the solution*

$$\begin{aligned}u(\mathbf{x},t) &= \frac{\partial}{\partial t} \frac{1}{4\pi c^2 t} \int\limits_{|\mathbf{y}|=ct} f(\mathbf{x}-\mathbf{y})\, \mathrm{d}o(\mathbf{y}) + \frac{1}{4\pi c^2 t} \int\limits_{|\mathbf{y}|=ct} g(\mathbf{x}-\mathbf{y})\, \mathrm{d}o(\mathbf{y}) \\ &= \frac{\partial}{\partial t} \frac{t}{4\pi} \int\limits_{|\mathbf{n}|=1} f(\mathbf{x}+ct\mathbf{n})\, \mathrm{d}o(\mathbf{n}) + \frac{t}{4\pi} \int\limits_{|\mathbf{n}|=1} g(\mathbf{x}+ct\mathbf{n})\, \mathrm{d}o(\mathbf{n}). \quad (12.8)\end{aligned}$$

For the integral transformation see p. 466. The assumptions on the initial conditions can be relaxed. If $f$ is three times and $g$ is twice continuously differentiable, it results in a classical solution $u$ that is twice continuously differentiable. The interchange of

differentiations and integrals made in (12.6) is allowed. The solution formula (12.8) shows that initial disturbances spread through space over time, and that with initial conditions $f$ and $g$ in $\mathcal{S}(\mathbb{R}^3)$ or those with bounded supports, the solution $u$ decays at least as fast as $1/t$ for increasing times $t$. The solution $u(\mathbf{x}, t)$ at a point $\mathbf{x}$ depends at time $t$ only on the values of the initial conditions on the spherical surface around $\mathbf{x}$ with radius $ct$. We also observe that $\delta(|\mathbf{x}| - ct)/(4\pi c^2 t)$ is a fundamental solution for inhomogeneous problems.

**Propagation of Local Disturbances.** *A spatially bounded initial disturbance leads to a time-limited effect in wave propagation in space.*

To explain this, we consider an initial disturbance whose support is a bounded set $U$ with the boundary surface $\partial U$. Then $f(\mathbf{x}) = g(\mathbf{x}) = 0$ outside of $U$. Specifically, imagine a sound that is generated in $U$ at time $t = 0$. Now, let $\mathbf{x}$ be a point outside of $U$ and $d$ and $D$ be the minimum and maximum distances between $\mathbf{x}$ and the points of $U$, respectively. For $t < d/c$, the sphere $S_{ct}(\mathbf{x})$ around $\mathbf{x}$ with radius $ct$ lies outside of $U$, $f$ and $g$ are zero there, and it follows that $u(\mathbf{x}, t) = 0$ for $t < d/c$. For $t = d/c$, $S_{ct}(\mathbf{x})$ touches the set $U$, the wave reaches $\mathbf{x}$: For times $t$ between $d/c$ and $D/c$, $S_{ct}(\mathbf{x})$ and $U$ intersect, at $\mathbf{x}$ effects $u(\mathbf{x}, t) \neq 0$ can occur. For times $t > D/c$, $U$ lies within the sphere $S_{ct}(\mathbf{x})$, and it follows again that $u(\mathbf{x}, t) = 0$, i.e., the disturbance has passed $\mathbf{x}$. Therefore, at $\mathbf{x}$ an effect $u(\mathbf{x}, t) \neq 0$ is noticeable only in the time interval $d/c \leqslant t \leqslant D/c$. There is a primary and a secondary wavefront. At a given time $t$, the primary wavefront takes the form of a surface that separates those points that have not yet been reached by the wave from the points where the disturbance is acting or has already acted. The points of this surface have a distance $ct$ from the boundary $\partial U$ of $U$, and thus lie on the envelope of all spheres with centers on $\partial U$ and radii $ct$ (*Huygens' principle*). Similarly, the secondary wavefront separates those points that are no longer affected by the disturbance from all others. The constant $c$ is the finite propagation speed of the wavefronts. To illustrate, consider the following Fig. 12.23 and Fig. 12.24.

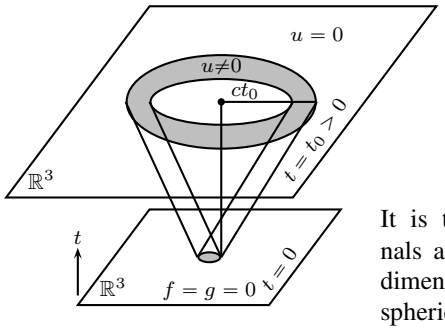


**Fig. 12.23.** Illustration of wave propagation in space

It is therefore possible to transmit signals as sharply bounded waves in three-dimensional space, whose support has a spherical or shell-like shape. This is an extremely significant fact for communication transmission.

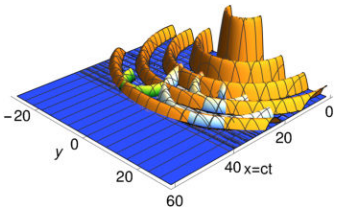


**Fig. 12.24.** Illustration of wave propagation and Huygens'principle

The second Fig. 12.24 illustrates a radial wave emitted by a sine source $A\sin(\omega t)s(t)$ at the origin. It shows the spatially decreasing amplitudes (for example air pressure or electric field strength) in the plane $0 < x = ct < 60, |y| \leqslant 30, z = 0$ for values $\geqslant 0$. The used data are $A = 1, \omega = \pi/2, c = 2$ with their according physical units. Shown is $u(x, y,0,20)$ at $t = 20$, when the wave has not yet reached $x > 40$. **Huygens' principle**: The wavefront can be seen as the envelope of the wave fronts by sources of the same type, but starting at different places and times before $t = 20$ with the correspondingly decreased amplitudes (blue, green in the figure for 2 such waves).

For the solution of the *inhomogeneous wave equation* $\Box u = \dfrac{1}{c^2}\partial_t^2 u - \Delta_{\mathbf{x}} u = f$ see Exercise A7. There we use the Lorentz gauge so that for an electric scalar potential $u$ we have $\Box u = \varrho/\varepsilon_0$ with the D'Alembert operator $\Box$. The result is the so-called *retarded potential*. The distribution $g_1(\mathbf{x}, t) = \delta(|x| - ct)/(4\pi c^2 t)$ in (12.7) is a fundamental solution of equation (12.5). Thus, it has to be multiplied by $c^2$ to obtain a fundamental solution $g$ for the D'Alembert operator $\Box$. With a twice continously differentiable source $f$, which is zero for $t < 0$, the retarded solution $f * g$ of $\Box u = f$ is also zero for $t < 0$, twice continuously differentiable, and can be written as integral (see also (9.4), p. 217. For the integrals, see p. 465 and Exercise A7)

$$u(\mathbf{x}, t) = f * \frac{\delta(|\mathbf{x}| - ct)}{4\pi t} = c^2 \int_{-\infty}^{t} \frac{(t-s)^2}{4\pi} \int_{|\mathbf{n}|=1} \frac{f(\mathbf{x} + c(t-s)\mathbf{n}, s)}{t-s} \, \mathrm{d}o(\mathbf{n}) \, \mathrm{d}s$$

$$= \int_{\mathbb{R}^3} \frac{f(\mathbf{y}, t - \frac{|\mathbf{x}-\mathbf{y}|}{c})}{4\pi|\mathbf{x}-\mathbf{y}|} \, \mathrm{d}\lambda^3(\mathbf{y}) = f * \frac{\delta(t - \frac{|\mathbf{x}|}{c})}{4\pi|\mathbf{x}|}. \tag{12.9}$$

The equations express mathematically precisely the Huygens principle (Fig. 12.24).

## The Initial Value Problem for the 2D Homogeneous Wave Equation

The wave equation in the plane describes problems where the initial conditions $f$ and $g$ depend only on two spatial coordinates. We consider functions $f$ that are three times continuously differentiable and functions $g$ that are twice continuously differentiable, which depend in $\mathbf{x} = (x_1, x_2, x_3)$ only on $x_1$ and $x_2$, interpret the corresponding initial value problem (12.5) in the plane as a spatial problem with the symmetry axis $x_1 = x_2 = 0$, and use its already known solution (12.8):

We calculate the surface integrals in (12.8) by setting $\varphi = f$ or $\varphi = g$ and integrating using spherical coordinates. Then for $\mathbf{x} = (x_1, x_2, x_3)$ and functions $\varphi(\mathbf{x}) = \varphi(x_1, x_2)$ independent of $x_3$ we have

$$\int\limits_{|\mathbf{n}|=1} \varphi(\mathbf{x}+ct\mathbf{n})\,\mathrm{d}o(\mathbf{n}) = \int\limits_0^{2\pi}\int\limits_0^{\pi} \varphi(x_1+ct\sin\theta\cos\phi, x_2+ct\sin\theta\sin\phi)\sin\theta\,\mathrm{d}\theta\,\mathrm{d}\phi\,.$$

We integrate over the upper and lower hemisphere surfaces separately, that is, we divide the integration range of the inner integral at $\pi/2$ into two subintervals. Using the substitution $\theta = \arcsin r$, $\mathrm{d}\theta = (1-r^2)^{-1/2}\,\mathrm{d}r$, it follows

$$\begin{aligned}&\int\limits_0^{\pi/2} \varphi(x_1 + ct\sin\theta\cos\phi, x_2 + ct\sin\theta\sin\phi)\sin\theta\,\mathrm{d}\theta\\ &= \int\limits_0^1 \frac{\varphi(x_1 + ctr\cos\phi, x_2 + ctr\sin\phi)}{\sqrt{1-r^2}} r\,\mathrm{d}r\,.\end{aligned}$$

For the second subintegral from $\pi/2$ to $\pi$ one obtains the same result. Substituting into the surface integral then gives for $\mathbf{x} = (x_1, x_2, x_3)$

$$\int\limits_{|\mathbf{n}|=1} \varphi(\mathbf{x}+ct\mathbf{n})\,\mathrm{d}o(\mathbf{n}) = 2\int\limits_0^{2\pi}\int\limits_0^{1} \frac{\varphi(x_1 + ctr\cos\phi, x_2 + ctr\sin\phi)}{\sqrt{1-r^2}} r\,\mathrm{d}r\,\mathrm{d}\phi\,.$$

This is an integral independent of $x_3$ over the unit disk in the $x_1x_2$-plane. So if $f$ and $g$ for $\mathbf{x} = (x_1, x_2, x_3)$ depend only on the first two coordinates, then the solution of the initial value problem (12.5) is also independent of $x_3$. Because the integrands are independent of the height $x_3$, the surface integrals in (12.8) can be expressed as two identical integrals over the unit disk in the plane $x_3 = 0$. Thus, we obtain the solution of the initial value problem (12.5) for planar problems and those with the symmetry axis $x_1 = x_2 = 0$.

**Theorem 12.8.** *The initial value problem (12.5) for the wave equation in the plane has the solution for* $\mathbf{x} = (x_1, x_2) \in \mathbb{R}^2$ *and* $t > 0$

$$u(\mathbf{x},t) = \frac{\partial}{\partial t}\frac{t}{2\pi}\int\limits_{|\mathbf{y}|\leqslant 1} \frac{f(\mathbf{x}+c t\mathbf{y})}{\sqrt{1-|\mathbf{y}|^2}}\,\mathrm{d}\lambda^2(\mathbf{y}) + \frac{t}{2\pi}\int\limits_{|\mathbf{y}|\leqslant 1} \frac{g(\mathbf{x}+c t\mathbf{y})}{\sqrt{1-|\mathbf{y}|^2}}\,\mathrm{d}\lambda^2(\mathbf{y})\,. \tag{12.10}$$

*For three-dimensional problems with the symmetry axis* $x_1 = x_2 = 0$*, the solution at time* $t > 0$ *at a point* $\mathbf{z} = (x_1, x_2, x_3) = (\mathbf{x}, x_3)$ *with* $u(\mathbf{z}, t) = u(\mathbf{x}, t)$ *is also given by formula (12.10).*

**Propagation of Local Disturbances.** *For the initial value problem of the wave equation in the plane, an initial disturbance bounded in space at any point leads to a timely unlimited effect.*

The solution $u$ at a point $\mathbf{x} = (x_1, x_2)$ in the plane depends at time $t > 0$ on the values of the initial conditions in the entire disk around $\mathbf{x}$ with radius $ct$. Local

disturbances in the plane propagate with the speed $c$ and then continuously affect points once reached by the wave. For example, if you place an autumn leaf on a still water surface and throw a stone into the water, the outgoing wave will reach the leaf and continue to spread. The leaf will continue to sway long after it has been passed by the propagation front. This may provide an illustration of the situation, even though water waves are only very roughly described by the two-dimensional wave equation (12.5). The difference to the previously discussed propagation of spatially local disturbances is easily understood when the planar problem is viewed as a three-dimensional problem with the symmetry axis $x_1 = x_2 = 0$. An initial condition with bounded support in the plane corresponds to a disturbance whose support is an infinitely extended cylinder in space. Even at arbitrarily large times, a point $(x_1, x_2)$ in the plane will be reached by disturbances from great heights $x_3$.

## The Initial Value Problem for the Homogeneous Heat Equation

The initial value problem for the homogeneous heat equation in homogeneous unbounded isotropic space is given for $u : \mathbb{R}^p \times [0, \infty[ \to \mathbb{R}$ by

$$\frac{\partial u}{\partial t}(\mathbf{x}, t) = k\Delta_{\mathbf{x}} u(\mathbf{x}, t)\,, \quad u(\mathbf{x},0) = f(\mathbf{x}). \tag{12.11}$$

Here, $u(\mathbf{x}, t)$ is the absolute temperature at a location $\mathbf{x} \in \mathbb{R}^p$ at time $t \geqslant 0$. The spatial dimension $p$ is arbitrary. The constant $k > 0$ is the thermal diffusivity. As with the wave equation, we initially assume the initial temperature $f \geqslant 0$ to be a smooth, rapidly decreasing function and obtain with the Fourier transform of the equations in (12.11) with respect to the spatial coordinates the ordinary differential equation

$$\frac{\partial \widehat{u}}{\partial t}(\boldsymbol{\omega}, t) = -k|\boldsymbol{\omega}|^2 \widehat{u}(\boldsymbol{\omega}, t)\,, \quad \widehat{u}(\boldsymbol{\omega},0) = \widehat{f}(\boldsymbol{\omega}).$$

Imposing $\widehat{u} = 0$ for $t < 0$ its unique solution is $\widehat{u}(\boldsymbol{\omega}, t) = \left(\widehat{f}(\boldsymbol{\omega})\, \mathrm{e}^{-k|\boldsymbol{\omega}|^2 t}\right) s(t)$. With the inverse Fourier transform $K_t(\mathbf{x}) = (4\pi kt)^{-p/2}\, \mathrm{e}^{-|\mathbf{x}|^2/(4kt)}$ of $\mathrm{e}^{-k|\boldsymbol{\omega}|^2 t}$ for $t > 0$ the solution of (12.11) follows by convolution of $f$ with $K_t$.

**Theorem 12.9.** *The initial value problem (12.11) for the homogeneous heat equation has for $\mathbf{x} \in \mathbb{R}^p$ and $t > 0$ the solution*

$$u(\mathbf{x}, t) = (4\pi kt)^{-p/2} \int_{\mathbb{R}^p} f(\mathbf{y})\, \mathrm{e}^{-|\mathbf{x}-\mathbf{y}|^2/(4kt)}\, \mathrm{d}\lambda^p(\mathbf{y})\,. \tag{12.12}$$

Due to the rapid decay of the heat kernel $K_t(\mathbf{x})$, a smooth solution still results for initial conditions $f \in \mathcal{S}'(\mathbb{R}^p)$. It can be proven (cf. for example F. John (1981)) that for $f \geqslant 0$, the solution $u$ in (12.12) is the unique non-negative solution of the heat problem (12.11). If until time $t = 0$ the temperature is zero everywhere and

at a location $\mathbf{y}$ at time $t = 0$ the temperature $f(\mathbf{y})$ is produced, then the density function $f(\mathbf{y})K_t(\mathbf{x}-\mathbf{y})$ describes the temperature in $\mathbf{x}$ at time $t$ produced at $\mathbf{y}$. The heat kernel thus shows the equalization of temperature spatially and temporally, the convolution integral (12.12) the superposition of the influences that act in $\mathbf{x}$ at time $t$ by the initial temperatures of all spatial points $\mathbf{y}$.

Inhomogeneous initial value problems for wave and heat equations in space can also be solved using the Fourier method. For this, one has to determine fundamental solutions of the equations. For the heat equation, this is posed as Exercise A6, for the 3D wave equation as Exercise A7, for the Schrödinger equation as Exercise A8 at the end of the chapter. For the 3D potential equation, we have already derived a fundamental solution on p. 216, in the 2D case in Exercise A7 of Chapter 9. Fundamental solutions to other problems can be found , for example, in H. Triebel (1992), L. Hörmander (2003), and N. Ortner, P. Wagner (2015).

## Inhomogeneous Boundary Value Problems for the Heat Equation

In applied numerical mathematics, inhomogeneous heat equations with various initial and boundary conditions for complex 3D-regions can approximately be solved with the Finite Element Method as introduced in Section 9.5. If the problems are time-dependent, one can also use it, when solutions are calculated in progressive discrete time steps. For theory on the (distributional) solutions for such problems it is referred to the extensive literature about partial differential equations and FEM methods, for example, to R. Dautray, J. L. Lions (1992).

As an example, the temperature distribution in a pump casing is shown, computed with Elmer FEM (see https://research.csc.fi/web/elmer). I have chosen this example because interested readers can easily reproduce it themselves, as the software and the data can be downloaded free of charge from the Elmer homepage. There can be found other examples too. Fig. 12.25 shows the used mesh.

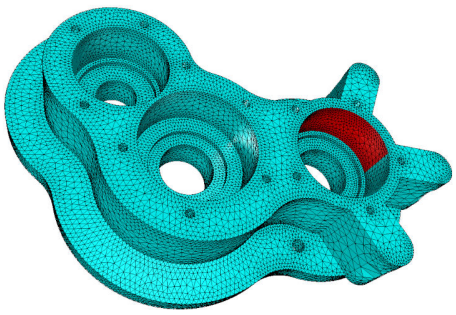

**Fig. 12.25.** 3D-FEM Model of a pump casing with the used mesh

Heat is being generated internally in the casing during operation and being cooled at parts of the upper boundary, providing a steady state temperature. Thus, no initial conditions were needed. Fig. 12.26 shows the approximate FEM solution. It is not differentiable and can only be understood as a weak solution in an appropriate Sobolev space (cf. p. 226). In the image, the surface of the model is smoothed. The solver needed 9 s on my old notebook to compute the solution.

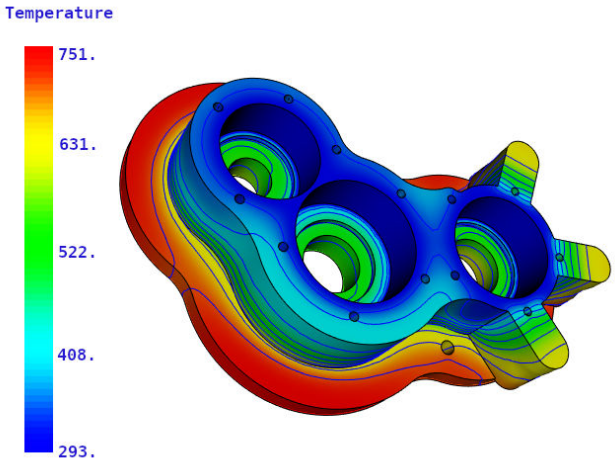


**Fig. 12.26.** Temperature in the pump casing generated during operation

The following input data have been used:

1. The model has 181214 volume elements and 58761 edge elements
2. The material is assumed to be aluminum
3. During operation the pump is cooled to 293K on parts of the upper surface
4. The inner heat source is assumed to be constant 0.017 W/kg. The temperature scale is given in degrees Kelvin, i.e., $293\text{K} = 19.85^\circ\text{C} = 67.73^\circ\text{F}$.

## 12.9 Exercises

**A1)** Assume that a function $f \in L^2(\mathbb{R})$ satisfies the conditions of the sampling theorem of p. 358 with $\widehat{f}(\omega) = 0$ for $|\omega| > \omega_c$. Furthermore, let $\alpha > 1$.

(a) Show that for $|\omega| \leqslant \alpha\omega_c$ the following holds:

$$\widehat{f}(\omega) = \frac{\pi}{\alpha\omega_c} \sum_{k=-\infty}^{+\infty} f\left(\frac{k\pi}{\alpha\omega_c}\right) \mathrm{e}^{-jk\pi\omega/(\alpha\omega_c)} .$$